
A Flexible, Equivariant Framework for Subgraph GNNs via Graph Products and Graph Coarsening

Guy Bar-Shalom

Computer Science
Technion - Israel Institute of Technology

Yam Eitan

Electrical & Computer Engineering
Technion - Israel Institute of Technology

Fabrizio Frasca

Electrical & Computer Engineering
Technion - Israel Institute of Technology

Haggai Maron

Electrical & Computer Engineering
Technion - Israel Institute of Technology
NVIDIA Research

Abstract

Subgraph Graph Neural Networks (Subgraph GNNs) enhance the expressivity of message-passing GNNs by representing graphs as sets of subgraphs. They have shown impressive performance on several tasks, but their complexity limits applications to larger graphs. Previous approaches suggested processing only subsets of subgraphs, selected either randomly or via learnable sampling. However, they make suboptimal subgraph selections or can only cope with very small subset sizes, inevitably incurring performance degradation. This paper introduces a new Subgraph GNNs framework to address these issues. We employ a graph coarsening function to cluster nodes into super-nodes with induced connectivity. The product between the coarsened and the original graph reveals an implicit structure whereby subgraphs are associated with specific sets of nodes. By running generalized message-passing on such graph product, our method effectively implements an efficient, yet powerful Subgraph GNN. Controlling the coarsening function enables meaningful selection of any number of subgraphs while, contrary to previous methods, being fully compatible with standard training techniques. Notably, we discover that the resulting node feature tensor exhibits new, unexplored permutation symmetries. We leverage this structure, characterize the associated linear equivariant layers and incorporate them into the layers of our Subgraph GNN architecture. Extensive experiments on multiple graph learning benchmarks demonstrate that our method is significantly more flexible than previous approaches, as it can seamlessly handle any number of subgraphs, while consistently outperforming baseline approaches.

1 Introduction

Subgraph GNNs [4, 12, 40, 8, 28, 30, 39, 3] have recently emerged as a promising direction in graph neural network research, addressing the expressiveness limitations of Message Passing Neural Networks (MPNNs) [24, 36, 25]. In essence, a Subgraph GNN operates on a graph by transforming it into a collection of subgraphs, generated based on a specific selection policy. For example, this could involve removing a single node from the original graph or simply marking a node without changing the graph’s original connectivity [27]. The model then processes these subgraphs using an equivariant architecture, aggregates the derived representations, and makes graph- or node-level predictions. The growing popularity of Subgraph GNNs stems not only from their enhanced expressive capabilities over MPNNs but also from their impressive empirical results, as notably demonstrated on well-known molecular benchmarks [39, 12, 3].

Unfortunately, Subgraph GNNs are hindered by substantial computational costs as they necessitate message-passing operations across all subgraphs within the bag. Typically, the number of subgraphs is the number of nodes in the graph, n , resulting in a time complexity scaling quadratically ($\mathcal{O}(n^2)$)

for bounded degree graphs, in contrast to a standard MPNN, whose time complexity is linear in the number of nodes for such graphs. This significant computational burden becomes impractical in large graphs, limiting the applicability of Subgraph GNNs to important applications and widely used datasets. To overcome this challenge, various studies have explored methodologies that process only a subset of subgraphs from the bag. These methods range from simple random sampling techniques [8, 4, 41, 3] to more advanced strategies that learn to select the most relevant subset of the bag to process [5, 20, 30]. However, while random sampling of subgraphs yields subpar performance, more sophisticated learnable selection strategies also have significant limitations. Primarily, they rely on discrete sampling during training, which can complicate the training process, as evidenced by the high number of epochs required to train them [20, 5, 30]. As a result, these methods often allow only a very small bag size, which only yields modest performance improvements compared to random sampling and standard MPNNs.

Our approach. The goal of this paper is to devise a Subgraph GNN architecture that can flexibly generate and process variable-sized subgraph policies, and deliver strong experimental results while sidestepping intricate and lengthy training protocols. Specifically, our approach aims to overcome the common limitation of restricting usage to a very small set of subgraphs.

Our proposed method builds upon and extends an observation made in [3], which draws an analogy between using Subgraph GNNs and performing message-passing operations over a larger “product graph”. Specifically, it was shown that when considering the maximally expressive Subgraph GNN suggested by [39], the bag of subgraphs and its update rules can be obtained by transforming a graph through

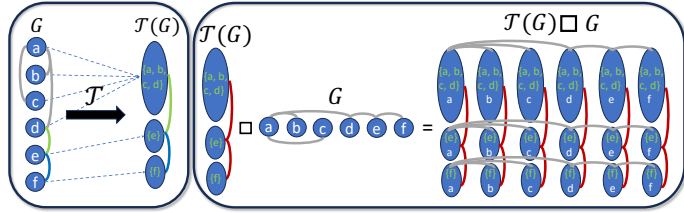


Figure 1: Product graph construction. **Left:** Transforming of the graph into a coarse graph; **Right:** Cartesian product of the coarsened graph with the original graph. The vertical axis corresponds to the subgraph dimension (super-nodes), while the horizontal axis corresponds to the node dimension (nodes).

the *graph cartesian product* of the original graph with itself, i.e. $G \square G$, and then processing this resulting graph using a standard MPNN. In our approach, we propose to modify the first term of the product and replace it with a *coarsened* version of the original graph, denoted $\mathcal{T}(G)$, obtained by mapping nodes to *super-nodes* (e.g., by applying graph clustering, see Figure 1(left)), making the resulting product graph $\mathcal{T}(G) \square G$ significantly smaller. This construction is illustrated in Figure 1(right). This process effectively associates each subgraph with a set of nodes, so that, by controlling the coarsening function, it allows for both flexible bag sizes and a simple, meaningful selection of the subgraphs.

While performing message passing on $\mathcal{T}(G) \square G$ serves as the core update rule in our architecture, we augment our message passing operations with another set of operations derived from the symmetry structure of the resulting node feature tensor, which we call *symmetry-based updates*. Specifically, the node feature tensor in our case is indexed by pairs (S, i) where S is a super-node and i is an original node. Accordingly, \mathcal{X} is a $2^n \times n \times d$ (very) sparse tensor, where 2^n is the number of all subsets of the vertex set, and d is the feature dimension. Interestingly, we find that this object adheres to a specific set of symmetries, which, to the best of our knowledge, is yet unstudied in the context of machine learning: applying permutation $\sigma \in S_n$ to the nodes in S and to i results in an equivalent representation of our node feature tensor. We formally define the symmetries of this object and characterize all the affine equivariant operations in this space. We incorporate these operations into our message-passing by encoding the parameter-sharing

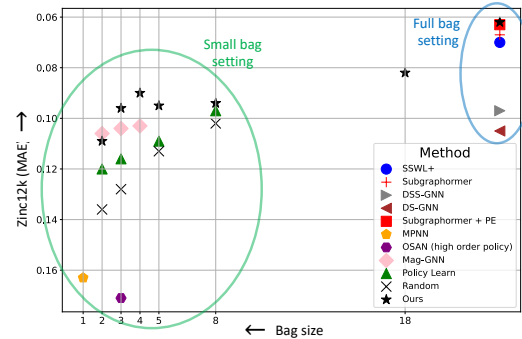


Figure 2: The performance landscape of Subgraph GNNs with varying number of subgraphs: Our method leads in the lower bag-size set, outperforming other approaches in nearly all cases. Additionally, our method matches the performance of state-of-the-art Subgraph GNNs in the full-bag setting. The full mean absolute error (MAE) scores along with standard deviations are available in Table 9 in the appendix.

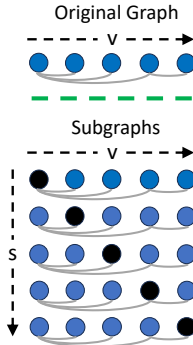
schemes [31] as additional edge features, and by deriving novel provably powerful node marking techniques for our setup. These additional update rules significantly improve experimental results. We note, that our symmetry analysis may be useful for processing bags derived from other high-order generation policies [30, 20] by treating tuples of nodes as sets.

The flexibility and effectiveness of our entire framework are illustrated in Figure 2, in which we performed a thorough experimental study on the popular ZINC-12K dataset [32]. Our method demonstrates a significant performance boost over baseline models in the *small bag* setting (the one they are designed for), while achieving results that compare favourably to state-of-the-art Subgraph GNNs in the *full bag* setting. Additionally, we can obtain results in-between these two regimes.

Contributions. The main contributions of this paper are: (1) the development of a novel, flexible Subgraph GNN framework that enables meaningful construction and processing of bags of subgraphs of any size; (2) a characterization of all affine invariant/equivariant layers defined on our node feature tensors; (3) a theoretical analysis of our method, demonstrating the expressivity benefits of our approach; (4) a comprehensive experimental evaluation demonstrating the advantages of the new approach across both small and large bag sizes, achieving state-of-the-art results, often by a significant margin.

2 Related work

Subgraph GNNs. Subgraph GNNs [40, 8, 28, 4, 41, 27, 12, 30, 17, 39, 3] represent a graph as a collection of subgraphs, obtained by a predefined generation policy. For example, each subgraph can be generated by marking exactly one node in the original graph (see inset ¹) – an approach commonly referred to as *node marking* [27]; this marked node is considered the root node in his subgraph. Several recent papers focused on scaling these methods to larger graphs, starting with basic random selection of subgraphs from the bag, and extending beyond with more sophisticated techniques that aim to learn how to select subgraphs. To elaborate, [5] introduced *Policy-Learn* (PL), an approach based on two models, where the first model predicts a distribution over the nodes of the original graph, and the second model processes bags of subgraphs sampled from this distribution. *MAG-GNN* [20] employs a similar approach utilizing reinforcement learning. Similarly to our approach, this method permits high-order policies by associating subgraphs with tuples rather than individual nodes, allowing for the marking of several nodes within a subgraph. However, as mentioned before, these approaches involve discrete sampling while training, making them very hard to train (1000-4000 epochs vs. ~ 400 epochs of state-of-the-art methods [3, 39] on the ZINC-12K dataset), and limiting their usage to very small bags. Finally, we mention another high-order method, *OSAN*, introduced by [30], which learns a distribution over tuples that represent subgraphs with multiple node markings. In the context of these works, our subgraph selection procedure can be seen as a variant of high-order policies, where instead of using ordered tuples, our subgraphs are indexed by subsets of indices. In contrast to these previous approaches, we suggest a simple and effective way to select subgraphs and also show how to leverage the resulting symmetry structure to augment our message-passing operations.



Symmetries in graph learning. Many previous works have analyzed and utilized the symmetry structure that arises from graph learning setups [22, 23, 18, 2]. Specifically relevant to our paper is the work of [22] that characterized basic equivariant linear layers for graphs, the work of [1] that characterizes equivariant maps for many other types of incidence tensors that arise in graph learning, and the recent works [4, 12] that leveraged group symmetries for designing Subgraph GNNs in a principled way.

3 Preliminaries

Notation. Let \mathcal{G} be a family of undirected graphs, and consider a graph $G = (V, E)$ within this family. The adjacency matrix $A \in \mathbb{R}^{n \times n}$ defines the connectivity of the graph², while the feature matrix $X \in \mathbb{R}^{n \times d}$ represents the node features. Here, V and E represent the sets of nodes and edges, respectively, with $|V| = n$ indicating the number of nodes. We use the notation $v_1 \sim_A v_2$ to

¹The Figure was taken with permission from [3]

²Edge features are omitted for simplicity.

denote that v_1 and v_2 are neighboring nodes according to the adjacency A . Additionally, we define $[n] \triangleq \{1, 2, \dots, n\}$, and $\mathcal{P}([n])$ as the power set of $[n]$.

Subgraph GNNs as graph products. In a recent work, [3] demonstrated that various types of update rules used by current Subgraph GNNs can be simulated by employing a *Cartesian graph product* between the original graph and another graph, and running standard message passing over that newly constructed product graph. Formally, the cartesian product of two graphs G_1 (n_1 nodes) and G_2 (n_2 nodes), denoted by $G_1 \square G_2$, forms a graph with vertex set $V(G_1) \times V(G_2)$. Two vertices (u_1, u_2) and (v_1, v_2) are adjacent if either $u_1 = v_1$ and u_2 is adjacent to v_2 in G_2 , or $u_2 = v_2$ and u_1 is adjacent to v_1 in G_1 . We denote by $\mathcal{A} \in \mathbb{R}^{n_1 \cdot n_2 \times n_1 \cdot n_2}$ and $\mathcal{X} \in \mathbb{R}^{n_1 \cdot n_2 \times d}$ the adjacency and node feature matrices of the product graph; in general, we use calligraphic letters to denote the adjacency and feature matrices of product graphs, while capital English letters are used for those of the original graphs. In particular, for the graph cartesian product, $G_1 \square G_2$, the following holds:

$$\mathcal{A}_{G_1 \square G_2} = A_1 \otimes I + I \otimes A_2. \quad (1)$$

For a detailed definition of the cartesian product of graphs, please refer to Definition A.1. As a concrete example for the analogy between Subgraph GNNs and the Cartesian product of graphs, we refer to a result by [3], which states that the maximally expressive Subgraph GNN architecture GNN-SSWL+ [39], can be simulated by an MPNN on the Cartesian product of the original graph with itself, denoted as $G \square G$. As we shall see, our framework utilizes a cartesian product of the original graph and a coarsened version of it, as illustrated in Figure 1 (right).

Equivariance. A function $L : V \rightarrow W$ is called equivariant if it commutes with the group action. More formally, given a group element, $g \in \mathbb{G}$, the function L should satisfy $L(g \cdot v) = g \cdot L(v)$ for all $v \in V$ and $g \in \mathbb{G}$. Invariance, a related concept, occurs when L satisfies $L(g \cdot v) = L(v)$.

4 Coarsening-based Subgraph GNN

Overview. This section introduces the Coarsening-based Subgraph GNN (CS-GNN) framework. The main idea is to select and process subgraphs in a principled and flexible manner through the following approach: (1) coarsen the original graph via a coarsening function, \mathcal{T} – see Figure 1(left); (2) Obtain the product graph – Figure 1(right) defined by the combination of two adjacencies, $\mathcal{A}_{\mathcal{T}(G)}$ (red edges), \mathcal{A}_G (grey edges), which arise from the graph Cartesian product operation (details follow); (3) leveraging the symmetry of this product graph to develop *symmetry-based* updates, described by $\mathcal{A}_{\text{Equiv}}$ (this part is not visualized in Figure 1). The general update of our suggested layer takes the following form³,

$$\mathcal{X}^{t+1}(S, v) = f^t \left(\underbrace{\{\mathcal{X}(S', v')^t\}_{(S', v') \sim \mathcal{A}_G(S, v)}}_{\text{Original connectivity (horizontal)}}, \underbrace{\{\mathcal{X}(S', v')^t\}_{(S', v') \sim \mathcal{A}_{\mathcal{T}(G)}(S, v)}}_{\text{Induced connectivity (vertical)}}, \underbrace{\{\mathcal{X}(S', v')^t\}_{(S', v') \sim \mathcal{A}_{\text{Equiv}}(S, v)}}_{\text{Symmetry-based updates}} \right), \quad (2)$$

where the superscript t indicates the layer index. In what follows, we further elaborate on these three steps (in Sections 4.1 to 4.2). We note, that each connectivity in Equation (2) is processed using a different MPNN, for more specific implementation details, we refer to Appendix F.

4.1 Product graph definition

As mentioned before, a maximally expressive Subgraph GNN can be realized via the Cartesian product of the original graph with itself $G \square G$. In this work, we extend this concept by allowing the left operand in the product to be the coarsened version of G , denoted as $\mathcal{T}(G)$, as defined next. This idea is illustrated in Figure 1.

Graph coarsening. Consider a graph $G = (V, E)$ with n nodes and an adjacency matrix A . Graph coarsening is defined by the function $\mathcal{T} : \mathcal{G} \rightarrow \mathcal{G}$, which maps G to a new graph $\mathcal{T}(G) = (V^{\mathcal{T}}, E^{\mathcal{T}})$ with an adjacency matrix $A^{\mathcal{T}} \in \mathbb{R}^{2^n \times 2^n}$ and a feature matrix $X^{\mathcal{T}} \in \mathbb{R}^{2^n \times d}$. Here, $V^{\mathcal{T}}$, the vertex set of the new graph represents super-nodes – defined as subsets of $[n]$. Additionally, we require

³Edge features are also allowed but are omitted here for simplicity.

that nodes in $V^{\mathcal{T}}$ induce a partition over the nodes of the original graph⁴. The connectivity $E^{\mathcal{T}}$ is extremely sparse and induced from the original graph’s connectivity via the following rule:

$$A^{\mathcal{T}}(S_1, S_2) = \begin{cases} 1 & \text{if } \exists v \in S_1, \exists v \in S_2 \text{ s.t. } A(v, u) = 1, \\ 0 & \text{otherwise,} \end{cases} \quad (3)$$

To clarify, in our running example (Figure 1), it holds that $A^{\mathcal{T}}(\{a, b, c, d\}, \{e\}) = 1$, while $A^{\mathcal{T}}(\{e\}, \{f\}) = 0$. For a more formal definition, refer to Definition A.3.

Our implementation of the graph coarsening function \mathcal{T} employs spectral clustering [34]⁵ to produce T clusters, which in our framework controls the size of the bag.

Defining $\mathcal{T}(G) \square G$. We define the connectivity of the product graph, see Figure 1(right), by applying the cartesian product between the coarsened graph, $\mathcal{T}(G)$, and the original graph, G . The product graph is denoted by $\mathcal{T}(G) \square G$, and is represented by the matrices $\mathcal{A}_{\mathcal{T}(G) \square G} \in \mathbb{R}^{(2^n \times n) \times (2^n \times n)}$ and $\mathcal{X} \in \mathbb{R}^{2^n \times n \times d}$ ⁶, where by recalling Equation (1), we obtain,

$$\mathcal{A}_{\mathcal{T}(G) \square G} = \overbrace{A^{\mathcal{T}} \otimes I}^{\triangleq \mathcal{A}_{\mathcal{T}(G)}} + \overbrace{I \otimes A}^{\triangleq \mathcal{A}_G}. \quad (4)$$

The connectivity in this product graph induces the horizontal (\mathcal{A}_G) and vertical updates ($\mathcal{A}_{\mathcal{T}(G)}$) in Equation (2), visualized in Figure 1(right) via grey and red redges, respectively.

4.2 Symmetry-based updates

In the previous subsection, we relied on a combination of a coarsening function and the graph Cartesian product to derive the two induced connectivities $\mathcal{A}_G, \mathcal{A}_{\mathcal{T}(G)}$ of our product graph. As mentioned before, these connectivities are used to perform message-passing on our product graph (see Equation (2)).

Inspired by recent literature on Subgraph GNNs [12, 3, 39], which incorporated and analyzed additional non-local updates arising from various symmetries (e.g., updating a node’s representation via all nodes in its subgraphs), this section aims to identify potential new updates that can be utilized over our product graph. More specifically, in this section we focus on the third term in Equation (2), dubbed *Symmetry-based updates*. To that end, we study the symmetry structure of the node feature tensor in our product graph, $\mathcal{X}(S, v)$. For better clarity in this derivation, we change the notation from nodes (v) to indices (i).

4.2.1 Symmetries of our product graph

Since the order of nodes in the original graph G is arbitrary, each layer in our architecture must exhibit equivariance to any induced changes in the product graph. This requires maintaining equivariance to permutations of nodes in both the original graph and its transformation $\mathcal{T}(G)$. As a result, recalling that $\mathcal{A} \in \mathbb{R}^{(2^n \times n) \times (2^n \times n)}$ and $\mathcal{X} \in \mathbb{R}^{2^n \times n \times d}$ represent the adjacency and feature matrices of the product graph, the symmetries of the product graph are defined by an action of the symmetric group S_n . Formally, a permutation $\sigma \in S_n$ acts on the adjacency and feature matrices by:

$$(\sigma \cdot \mathcal{A})(S_1, i_1, S_2, i_2) = \mathcal{A}(\sigma^{-1}(S_1), \sigma^{-1}(i_1), \sigma^{-1}(S_2), \sigma^{-1}(i_2)), \quad (5)$$

$$(\sigma \cdot \mathcal{X})(S, i) = \mathcal{X}(\sigma^{-1}(S), \sigma^{-1}(i)), \quad (6)$$

where we define the action of $\sigma \in S_n$ on a set $S = \{i_1, i_2, \dots, i_k\}$ of size k as: $\sigma \cdot S \triangleq \{\sigma^{-1}(i_1), \sigma^{-1}(i_2), \dots, \sigma^{-1}(i_k)\} \triangleq \sigma^{-1}(S)$.

⁴Our method also supports the case of which it is not a partition.

⁵Other graph coarsening or clustering algorithms can be readily used as well.

⁶We note that while the node matrix of the product graph, \mathcal{X} , can be initialized in various ways, e.g., deep sets-based architecture [38], in our implementation we simply use the original node features, i.e., $\mathcal{X}(S, v) = X(v)$, given that X is the node feature matrix of the original graph.

4.2.2 Derivation of linear equivariant layers for the node feature tensor

Here we will characterize the linear equivariant layers with respect to the symmetry defined above, focusing on Equation (6). We adopt a similar notation to [22], and note that, in our derivation, we assume for simplicity that the number of feature channels is $d = 1$ (extension to multiple features is straightforward [22]). In addition, our analysis considers the more general case where V^T encompasses all potential super-nodes formed by subsets of $[n]$.

Our main tool is the characterization of linear equivariant layers for permutation symmetries as parameter-sharing schemes [35, 31, 22]. In a nutshell, this characterization states that the parameter vectors of the biases, invariant layers, and equivariant layers can be expressed as a learned weighted sum of basis tensors, where the basis tensors are indicators of the orbits induced by the group action on the respective index spaces. We focus here on presenting the final results; detailed discussion and derivations are available in Appendix E. Our main results are summarized in Proposition E.1.

Equivariant bias and invariant layers. The bias vectors as well as the weight vectors defining linear layers in our space are in $\mathbb{R}^{2^n \times n}$. Hence, we define an equivalence relation \sim in the associated index space $\{1, \dots, 2^n \times n\}$ which, as stated before, corresponds to the orbits under the action of S_n . For pairs $(S, i) \in (\mathcal{P}([n]) \times [n])$, γ^{k+} corresponds to all pairs with $|S| = k$ and $i \notin S$, and γ^{k-} to all pairs with $|S| = k$ and $i \in S$, leading to the following partition:

$$(\mathcal{P}([n]) \times [n]) / \sim \triangleq \{\gamma^{k*} : k = 1, \dots, n; * \in \{+, -\}\}. \quad (7)$$

This partition effectively splits the indices (S, i) according to the size of S and whether $i \in S$. Given $\gamma \in (\mathcal{P}([n]) \times [n]) / \sim$, the following is a basis tensor of the bias vector of the invariant layer,

$$\mathbf{B}_{S,i}^\gamma = \begin{cases} 1, & \text{if } (S, i) \in \gamma; \\ 0, & \text{otherwise.} \end{cases} \quad (8)$$

Weight matrices. Following similar reasoning, consider elements $(S_1, i_1, S_2, i_2) \in (\mathcal{P}([n]) \times [n] \times \mathcal{P}([n]) \times [n])$. To characterize the orbits of S_n in this space we define partitions according to six conditions. For example, two of these conditions are the sizes of S_1 and S_2 , which remain invariant under permutations. Another condition is the size of the intersection set $S_1 \cap S_2$, which also remains invariant under permutations. For a thorough discussion and derivation of the six conditions, please refer to Appendix E. We define \sim as the equivalence relation for these six conditions. Given an equivalence class, or orbit, $\Gamma \in (\mathcal{P}([n]) \times [n] \times \mathcal{P}([n]) \times [n]) / \sim$, we define a basis tensor, $\mathbf{B}^\Gamma \in \mathbb{R}^{2^n \times n \times 2^n \times n}$ by setting:

$$\mathbf{B}_{S_1, i_1; S_2, i_2}^\Gamma = \begin{cases} 1, & \text{if } (S_1, i_1, S_2, i_2) \in \Gamma; \\ 0, & \text{otherwise.} \end{cases} \quad (9)$$

A visualization of the two basis vectors, Equations (8) and (9), is available in Figure 3. The following (informal) proposition summarizes the results in this section (the proof is given in Appendix G),

Proposition 4.1 (Basis of Invariant (Equivariant) Layers). *The tensors \mathbf{B}^γ (\mathbf{B}^Γ) in Equation (8) (Equation (9)) form an orthogonal basis (in the standard inner product) of the invariant layers and biases (Equivariant layers – weight matrix).*

4.2.3 Incorporating symmetry-based updates in our framework

In the previous subsection, we derived all possible linear invariant and equivariant operations that respect the symmetries of our product graph. We now use this derivation to define the symmetry-based

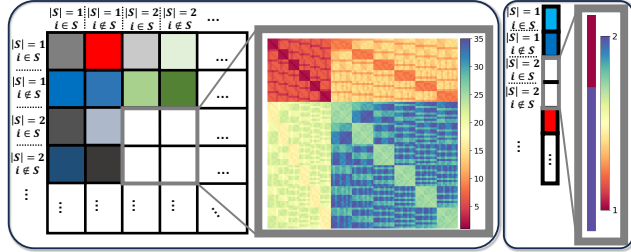


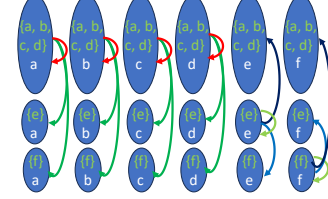
Figure 3: Visualization via heatmaps (different colors correspond to different parameters) of the parameter-sharing scheme determined by symmetries for a graph with $n = 6$ nodes, zooming-in on the block which corresponds to sets of size two. **Left:** Visualization of the weight matrix for the equivariant basis $\mathbf{B}_{S_1, i_1; S_2, i_2}^\Gamma$ (a total of 35 parameters in the block). **Right:** Visualization of the bias vector for the invariant basis $\mathbf{B}_{S,i}^\gamma$ (a total of 2 parameters in the block). Symmetry-based updates reduce parameters more effectively than previously proposed linear equivariant layers by treating indices as unordered tuples (see Appendix E.3 for a discussion).

updates in Equation (2), which correspond to the construction of $\mathcal{A}_{\text{Equiv}}$ and the application of an MPNN.

To begin, we note that any linear equivariant layer can be realized through an MPNN [13] applied to a fully connected graph with appropriate edge features. This is formally stated in Lemma F.1, the main idea is to encode the parameters on the edges of this graph (see visualization inset). Thus, the natural construction of $\mathcal{A}_{\text{Equiv}}$ corresponds to a fully connected graph, with appropriate edge features derived from the parameter-sharing scheme we have developed.

$$x_i = \sum_j w_{ij} x_j \iff \text{graph with nodes } i, j \text{ and edge weight } w_{ij}$$

However, one of our main goals and guidelines in developing our flexible framework is to maintain efficiency, and to align with the maximally expressive GNN, namely GNN-SSWL+ [39, 3], for the case of a trivial coarsening function, $\mathcal{T}(G) = G$ (which correspond to the full-bag setting). To achieve this, we opt for a sparser choice by using only a subset of the basis vectors (defined in Equation (9)) to construct $\mathcal{A}_{\text{Equiv}}$. Specifically, the matrix $\mathcal{A}_{\text{Equiv}}$ corresponding to the chosen subset of basis vectors is visualized inset. To clarify, the nodes (S, v) that satisfy $v \in S$ “send messages” (i.e., broadcast their representation) to all the nodes (S', v') such that $v = v'$. In Section 5, we discuss in greater detail how this relates to GNN-SSWL+. A more formal discussion regarding our implementation of those symmetry based updates is given in Appendix F.4.



Maintaining sparsity. We note that while our characterization considers all nodes $(S, v) \in (\mathcal{P}([n]) \times [n])$, in our specific choice of updates, we applied the updates only to the very sparse set of nodes in our product graph, i.e., $\mathcal{T}(G) \square G$. Nevertheless, this sparse update rule still preserves equivariance. This can be justified by applying a sparsity mask to exclude nodes not in the product graph before applying the linear equivariant layer over the full set of nodes. See discussion in [1].

Node Marking. While the bias term of the equivariant linear layer is the most natural choice to mark nodes in the product graph [26, 4, 12], our theoretical analysis in the next section reveals a more expressive variant, defined as follows,

$$\mathcal{X}_{S,i} \leftarrow \sum_{j \in S} z_{\text{SPD}(i,j)} \quad (10)$$

where $\text{SPD}(i, j)$ denotes the *shortest path distance* between nodes i and j in the original G^7 . Note that replacing the sum in Equation (10) with any other invariant aggregator maintains equivariance.

Pooling. After a stacking of layers of the form Equation (2), we employ a pooling layer⁸ to obtain a graph representation; switching back to the original notation (from indices i to nodes v) that is, $\rho(\mathcal{X}^T) = \text{MLP}^T \left(\sum_S \left(\sum_{v=1}^n \mathcal{X}^T(S, v) \right) \right)$; T denotes the final layer.

5 Theoretical analysis

In this section, we study several theoretical properties of our framework. We start by analyzing different node marking strategies and then discuss the relation between our method, Subgraph GNNs, and coarsening-based approaches. Here, we present only the main results, further discussion is available in Appendices B to D, proofs in Appendix G.

Node marking strategies. The employed node-marking strategy described in Equation (10) constitutes a reasonable, yet specific design choice, but other compelling alternatives are possible. Here we suggest four natural marking variants and compare them in their expressiveness: **Simple Node Marking** π_S : element (S, v) is ‘marked’ iff node v is in super-node S ; **Node + Size Marking** π_{SS} : element (S, v) is ‘marked’ according to π_S and, jointly, in a way to encode the size of S ; **Minimum Distance** (π_{MD}): element (S, v) is ‘marked’ with the minimum SPD between v and the nodes in S ; **Learned Distance Function** π_{LD} (Equation (10)): element (S, v) is ‘marked’ by evaluating a (learned) permutation invariant function over the set of SPDs between v and the nodes in S .

⁷To facilitate this, we maintain a lookup table where each index corresponds to a shortest path distance, assigning a learnable embedding, $z_{\text{SPD}(i,j)} \in \mathbb{R}^d$, to each node (S, i) .

⁸We note that for some of the theoretical analysis, we use: $\rho(\mathcal{X}^T) = \text{MLP}^T \left(\sum_S \left(\text{MLP}^T \left(\sum_{v=1}^n \mathcal{X}^T(S, v) \right) \right) \right)$

All the above variants represent natural extensions of the traditional marking techniques discussed in [4, 12, 27, 41], and constitute equally valid strategies for Higher-Order Subgraph GNNs operating on “unordered k-vertex subgraphs” [30, 27], which may be practically preferred to their ordered counterparts for efficiency reasons⁹. We conveniently gather the first three strategies as $\Pi = \{\pi_S, \pi_{SS}, \pi_{MD}\}$ and summarize the relation between all variants as follows:

Proposition 5.1 (Informal – Expressivity of marking strategies.). *(i) Strategies in Π are all equally expressive, independently of the transformation function \mathcal{T} . Also, they are as expressive as uniquely encoding the elements’ orbit (as per Section 4.2.1, Lemma E.1). (ii) The strategy π_{LD} is at least as expressive as strategies in Π . Additionally, there exists transformation functions s.t. it is strictly more expressive than all of them.*

The above are formally stated in Propositions C.1 to C.3, and more thoroughly discussed in Appendix C. Importantly, they give theoretical justification to our specific choice of π_{LD} (Equation (10)). This is notably in contrast with the setting of node-based, full-bag Subgraph GNNs, where SPD-based techniques are generally as expressive as traditional node-marking [3, 39].

Recovering maximally expressive Subgraph GNNs An advantage of our approach is that the transformation function \mathcal{T} can precisely control the behavior of our Subgraph GNN, allowing us to seamlessly interpolate between trivial message-passing equivalents on the original graph and maximally expressive node-based Subgraph GNNs, or to implement some higher-order variants thereof. The result below is formally stated in Proposition D.1 and further discussed in Appendix D.1:

Proposition 5.2 (Informal – Recovering the maximally expressive Subgraph GNNs). *For a trivial transformation function, namely $\mathcal{T}(G) = G$, CS-GNN can implement a maximally expressive Subgraph GNN as per [39].*

More than a coarsening function. Our approach’s effectiveness comes not just from transforming the input graph ($\mathcal{T}(G)$), but from our carefully designed equivariant layers. These layers enable effective processing of the new product graph $\mathcal{T}(G) \square G$, capturing information from both $\mathcal{T}(G)$ and G in a structured manner. We compare our method to a baseline that uses message-passing on the *sum graph*: the union of $\mathcal{T}(G)$ and G , with edges indicating node membership in super-nodes (defined formally in Definition D.2). We prove the following informal proposition, which we state formally in Propositions D.2 and D.3:

Proposition 5.3 (Informal – CS-GNN beyond coarsening). *For any transformation function \mathcal{T} , CS-GNN can implement message-passing on the sum graph, hence being at least as expressive. Also, there exist transformations \mathcal{T} ’s s.t. CS-GNN is strictly more expressive than that.*

6 Experiments

We experimented extensively over seven different datasets to answer the following questions: (Q1) Can CS-GNN outperform efficient Subgraph GNNs operating on small bags? (Q2) Does the additional symmetry-based updates boost performance? (Q3) Does CS-GNN in the full-bag setting validate its theory and match state-of-the-art full-bag Subgraph GNNs? (Q4) Does CS-GNN in the full-bag setting validate its theory and match state-of-the-art full-bag Subgraph GNNs?

In the following sections, we present our main results and refer to Appendix F for additional experiments and details.

Baselines. For each task, we include several baselines. The RANDOM baseline corresponds to random subgraph selection. We report the best performing random baseline from all prior work [5, 20, 30, 3]. The other two (non-random) baselines are: (1) LEARNED [5, 20, 30], which represents methods that learn the specific subgraphs to be used; and (2) FULL [39, 3], which corresponds to full-bag Subgraph GNNs.

Table 1: Results on ZINC-12K dataset. Top two results are reported as **First** and **Second**.

Method	Bag size	ZINC (MAE ↓)
GIN [36]	$T = 1$	0.163 ± 0.004
OSAN [30]	$T = 2$	0.177 ± 0.016
Random [20]	$T = 2$	0.131 ± 0.005
PL [5]	$T = 2$	0.120 ± 0.003
Mag-GNN [20]	$T = 2$	0.106 ± 0.014
Ours	$T = 2$	0.109 ± 0.005
Random [20]	$T = 3$	$0.124 \pm N/A$
Mag-GNN [20]	$T = 3$	$0.104 \pm N/A$
Ours	$T = 3$	0.096 ± 0.005
Random [20]	$T = 4$	$0.125 \pm N/A$
Mag-GNN [20]	$T = 4$	$0.101 \pm N/A$
Ours	$T = 4$	0.090 ± 0.003
Random [5]	$T = 5$	0.113 ± 0.006
PL [5]	$T = 5$	0.109 ± 0.005
Ours	$T = 5$	0.095 ± 0.003
GNN-SSWL+ [39]	Full	0.070 ± 0.005
Subgraphormer [3]	Full	0.067 ± 0.007
Subgraphormer+PE [3]	Full	0.063 ± 0.001
Ours	Full	0.062 ± 0.007

⁹In practice, all these marking strategies can be implemented via Embedding Lookup layers.

ZINC. We experimented with both the ZINC-12K and ZINC-FULL datasets [32, 14, 10], adhering to a 500k parameter budget as prescribed. As shown in Table 1, CS-GNN outperforms all efficient baselines by a significant margin, with at least a +0.008 MAE improvement for bag sizes $T \in \{3, 4, 5\}$. Additionally, in the full-bag setting, our method recovers state-of-the-art results. The results for ZINC-FULL are available in Table 8 in the Appendix.

OGB. We tested our framework on several datasets from the OGB benchmark collection [16]. Table 4 shows the performance of our method compared to both efficient and full-bag Subgraph GNNs. Our CS-GNN outperforms all baselines across all datasets for bag sizes $T \in \{2, 5\}$, except for the MOLHIV dataset with $T = 2$, where PL achieves the best results and our method ranks second. In the full-bag setting, CS-GNN is slightly outperformed by the top-performing Subgraph GNNs but still offers comparable results.

Peptides. We experimented on the PEPTIDES-FUNC and PEPTIDES-STRUCT datasets [9] – which full-bag Subgraph GNNs already struggle to process – evaluating CS-GNN’s ability to scale to larger graphs. The results are summarized in Table 2. By using an effective subset of subgraphs, CS-GNN outperforms all MPNN variants, even when incorporating structural encodings such as GAT-EDGCN+RWSE. Additionally, our method surpasses the random¹⁰ baseline on both datasets.

Table 2: Results on PEPTIDES dataset.

Model ↓ / Dataset →	PEPTIDES-FUNC (AP ↑)	PEPTIDES-STRUCT (MAE ↓)
GCN [19]	0.5930±0.0023	0.3496±0.0013
GIN [36]	0.5498±0.0079	0.3547±0.0045
GatedGCN [7]	0.5864±0.0077	0.3420±0.0013
GatedGCN+RWSE [9]	0.6069±0.0035	0.3357±0.0006
Random [3]	0.5924±0.005	0.2594±0.0021
Ours	0.6156±0.0080	0.2539±0.0015

Ablation study – symmetry-based updates. We assessed the impact of the symmetry-based update on the performance of CS-GNN. Specifically, we asked, *do the symmetry-based updates significantly contribute to the performance of CS-GNN?* To evaluate this, we conducted several experiments using the ZINC-12K dataset across various bag sizes, $T \in \{2, 3, 4, 5\}$, comparing CS-GNN with and without the symmetry-based update. The results are summarized in Table 3. It is clear that the symmetry-based updates play a key role in the performance of CS-GNN. For a bag size of $T = 2$, the inclusion of the symmetry-based update improves the MAE by a significant 0.34. For other bag sizes, the improvements range from 0.05 to 0.016, clearly demonstrating the benefits of including the symmetry-based updates.

Table 3: Ablation study.

Bag size	w/	w/o
T=2	0.109±0.005	0.143±0.003
T=3	0.096±0.005	0.101±0.006
T=4	0.090±0.003	0.106±0.001
T=5	0.095±0.003	0.104±0.005

Discussion. In what follows, we address research questions **Q1** to **Q4**. (A1) Tables 1, 2 and 4 clearly demonstrate that we outperform efficient Subgraph GNNs (which operate on a small bag) in 10 out of 12 dataset and bag size combinations. (A2) Our ablation study on the ZINC-12K dataset, as shown in Table 3, clearly demonstrates the benefits of the symmetry-based updates across all the considered bag sizes. (A3) Table 2 demonstrates that CS-GNN provides an effective solution when the full-bag setting cannot be applied, outperforming all baselines. (A4) On the ZINC-12K dataset (see Table 1), CS-GNN achieves state-of-the-art results compared to Subgraph GNNs. On the OGBG datasets (see Table 4), our performance is comparable to these top-performing Subgraph GNNs.

Table 4: Results on OGB datasets. The top two results are reported as **First** and **Second**.

Model ↓ / Dataset →	Bag size	MOLHIV (ROC-AUC ↑)	MOLBACE (ROC-AUC ↑)	MOLESOL (RMSE ↓)
GIN [36]	$T = 1$	75.58±1.40	72.97±4.00	1.173±0.057
Random [5]	$T = 2$	77.55±1.24	75.36±4.28	0.951±0.039
PL [5]	$T = 2$	79.13±0.60	78.40±2.85	0.877±0.029
Mag-GNN [20]	$T = 2$	77.12±1.13	-	-
Ours	$T = 2$	77.72±0.76	80.58±1.04	0.850±0.024
OSAN [30]	$T = 3$	-	-	0.959±0.184
OSAN [30]	$T = 5$	-	76.30±3.00	-
PL [5]	$T = 5$	78.49±1.01	78.39±2.28	0.883±0.032
Random [5]	$T = 5$	77.30±2.56	78.14±2.36	0.900±0.032
Ours	$T = 5$	79.09±0.90	79.64±1.43	0.863±0.029
GNN-SSWL+ [39]	Full	79.58±0.35	82.70±1.80	0.837±0.019
Subgraphormer	Full	80.38±1.92	81.62±3.55	0.832±0.043
Subgraphormer + PE	Full	79.48±1.28	84.35±0.65	0.826±0.010
Ours	Full	79.44±0.87	80.71±1.76	0.814±0.021

7 Conclusions

In this work, we employed graph coarsenings and leveraged the insightful connection between Subgraph GNNs and the graph Cartesian product to devise CS-GNN, a novel and flexible Subgraph GNN that can effectively generate and process any desired bag size. Several directions for future research remain open. Firstly, we experimented with spectral clustering based coarsening, but other

¹⁰For the PEPTIDES datasets, we benchmarked our model against the random variant of Subgraphormer + PE, which similarly incorporates information from the Laplacian eigenvectors. To ensure a fair comparison, we used a single vote. Additionally, since Subgraphormer + PE employs GAT [33] as the underlying MPNN, we also utilized GAT for this specific experiment to maintain consistency and fairness.

strategies are possible and are interesting to explore. Secondly, in our symmetry-based updates, we have only considered a portion of the whole equivariant basis we derived: evaluating the impact of other basis elements deserve further attention, both theoretically and in practice. Finally, whether Higher-Order Subgraph GNNs can benefit from our developed parameter-sharing scheme remains an intriguing open question.

Limitations. Our method operates over a product graph. Although we provide control over the size of this product graph, achieving higher performance requires a larger bag size. This can become a complexity bottleneck, particularly when the original graph is large.

Acknowledgements

The authors are grateful to Beatrice Bevilacqua, for helpful discussions, and constructive conversations about the experiments. HM is the Robert J. Shillman Fellow and is supported by the Israel Science Foundation through a personal grant (ISF 264/23) and an equipment grant (ISF 532/23). FF is funded by the Andrew and Erna Finci Viterbi Post-Doctoral Fellowship.

References

- [1] Marjan Albooyeh, Daniele Bertolini, and Siamak Ravanbakhsh. Incidence networks for geometric deep learning. *arXiv preprint arXiv:1905.11460*, 2019.
- [2] Waiss Azizian and Marc Lelarge. Expressive power of invariant and equivariant graph neural networks. *arXiv preprint arXiv:2006.15646*, 2020.
- [3] Guy Bar-Shalom, Beatrice Bevilacqua, and Haggai Maron. Subgraphormer: Unifying subgraph gnns and graph transformers via graph products, 2024.
- [4] Beatrice Bevilacqua, Fabrizio Frasca, Derek Lim, Balasubramaniam Srinivasan, Chen Cai, Gopinath Balamurugan, Michael M Bronstein, and Haggai Maron. Equivariant subgraph aggregation networks. *International Conference on Learning Representations*, 2022.
- [5] Beatrice Bevilacqua, Moshe Eliasof, Eli Meir, Bruno Ribeiro, and Haggai Maron. Efficient subgraph gnns by learning effective selection policies. *International Conference on Learning Representations*, 2024.
- [6] Lukas Biewald. Experiment tracking with weights and biases, 2020. URL <https://www.wandb.com/>. Software available from wandb.com.
- [7] Xavier Bresson and Thomas Laurent. Residual gated graph convnets. *arXiv preprint arXiv:1711.07553*, 2017.
- [8] Leonardo Cotta, Christopher Morris, and Bruno Ribeiro. Reconstruction for powerful graph representations. In *Advances in Neural Information Processing Systems*, volume 34, 2021.
- [9] Vijay Prakash Dwivedi, Ladislav Rampásek, Michael Galkin, Ali Parviz, Guy Wolf, Anh Tuan Luu, and Dominique Beaini. Long range graph benchmark. *Advances in Neural Information Processing Systems*, 35:22326–22340, 2022.
- [10] Vijay Prakash Dwivedi, Chaitanya K Joshi, Anh Tuan Luu, Thomas Laurent, Yoshua Bengio, and Xavier Bresson. Benchmarking graph neural networks. *Journal of Machine Learning Research*, 24(43):1–48, 2023.
- [11] Matthias Fey and Jan Eric Lenssen. Fast graph representation learning with pytorch geometric. *arXiv preprint arXiv:1903.02428*, 2019.
- [12] Fabrizio Frasca, Beatrice Bevilacqua, Michael Bronstein, and Haggai Maron. Understanding and extending subgraph gnns by rethinking their symmetries. *Advances in Neural Information Processing Systems*, 35:31376–31390, 2022.
- [13] Justin Gilmer, Samuel S Schoenholz, Patrick F Riley, Oriol Vinyals, and George E Dahl. Neural message passing for quantum chemistry. In *International conference on machine learning*, pages 1263–1272. PMLR, 2017.
- [14] Rafael Gómez-Bombarelli, Jennifer N Wei, David Duvenaud, José Miguel Hernández-Lobato, Benjamín Sánchez-Lengeling, Dennis Sheberla, Jorge Aguilera-Iparraguirre, Timothy D Hirzel, Ryan P Adams, and Alán Aspuru-Guzik. Automatic chemical design using a data-driven continuous representation of molecules. *ACS central science*, 4(2):268–276, 2018.
- [15] Weihua Hu, Bowen Liu, Joseph Gomes, Marinka Zitnik, Percy Liang, Vijay Pande, and Jure Leskovec. Strategies for pre-training graph neural networks. *arXiv preprint arXiv:1905.12265*, 2019.
- [16] Weihua Hu, Matthias Fey, Marinka Zitnik, Yuxiao Dong, Hongyu Ren, Bowen Liu, Michele Catasta, and Jure Leskovec. Open graph benchmark: Datasets for machine learning on graphs. *Advances in neural information processing systems*, 33:22118–22133, 2020.
- [17] Yinan Huang, Xingang Peng, Jianzhu Ma, and Muhan Zhang. Boosting the cycle counting power of graph neural networks with i^2 -gnns. In *The Eleventh International Conference on Learning Representations*, 2022.

- [18] Nicolas Keriven and Gabriel Peyré. Universal invariant and equivariant graph neural networks. *Advances in Neural Information Processing Systems*, 32, 2019.
- [19] Thomas N Kipf and Max Welling. Semi-supervised classification with graph convolutional networks. *International Conference on Learning Representations*, 2016.
- [20] Lecheng Kong, Jiarui Feng, Hao Liu, Dacheng Tao, Yixin Chen, and Muhan Zhang. Mag-gnn: Reinforcement learning boosted graph neural network. *Advances in Neural Information Processing Systems*, 36, 2024.
- [21] Jungmin Kwon, Jeongseop Kim, Hyunseo Park, and In Kwon Choi. Asam: Adaptive sharpness-aware minimization for scale-invariant learning of deep neural networks. In *International Conference on Machine Learning*, 2021.
- [22] Haggai Maron, Heli Ben-Hamu, Nadav Shamir, and Yaron Lipman. Invariant and equivariant graph networks. *arXiv preprint arXiv:1812.09902*, 2018.
- [23] Haggai Maron, Heli Ben-Hamu, Hadar Serviansky, and Yaron Lipman. Provably powerful graph networks. *Advances in neural information processing systems*, 32, 2019.
- [24] Christopher Morris, Martin Ritzert, Matthias Fey, William L Hamilton, Jan Eric Lenssen, Gaurav Rattan, and Martin Grohe. Weisfeiler and leman go neural: Higher-order graph neural networks. In *Proceedings of the AAAI conference on artificial intelligence*, volume 33, pages 4602–4609, 2019.
- [25] Christopher Morris, Yaron Lipman, Haggai Maron, Bastian Rieck, Nils M Kriege, Martin Grohe, Matthias Fey, and Karsten Borgwardt. Weisfeiler and leman go machine learning: The story so far. *arXiv preprint arXiv:2112.09992*, 2021.
- [26] Pál András Papp and Roger Wattenhofer. A theoretical comparison of graph neural network extensions. *CoRR*, abs/2201.12884, 2022.
- [27] Pál András Papp and Roger Wattenhofer. A theoretical comparison of graph neural network extensions. In *International Conference on Machine Learning*, pages 17323–17345. PMLR, 2022.
- [28] Pál András Papp, Karolis Martinkus, Lukas Faber, and Roger Wattenhofer. Dropgnn: Random dropouts increase the expressiveness of graph neural networks. *Advances in Neural Information Processing Systems*, 34:21997–22009, 2021.
- [29] Adam Paszke, Sam Gross, Francisco Massa, Adam Lerer, James Bradbury, Gregory Chanan, Trevor Killeen, Zeming Lin, Natalia Gimelshein, Luca Antiga, et al. Pytorch: An imperative style, high-performance deep learning library. *Advances in neural information processing systems*, 32, 2019.
- [30] Chendi Qian, Gaurav Rattan, Floris Geerts, Mathias Niepert, and Christopher Morris. Ordered subgraph aggregation networks. *Advances in Neural Information Processing Systems*, 35: 21030–21045, 2022.
- [31] Siamak Ravanbakhsh, Jeff Schneider, and Barnabas Poczos. Equivariance through parameter-sharing. In *International conference on machine learning*, pages 2892–2901. PMLR, 2017.
- [32] Teague Sterling and John J Irwin. Zinc 15–ligand discovery for everyone. *Journal of chemical information and modeling*, 55(11):2324–2337, 2015.
- [33] Petar Veličković, Guillem Cucurull, Arantxa Casanova, Adriana Romero, Pietro Lio, and Yoshua Bengio. Graph attention networks. *International Conference on Learning Representations*, 2017.
- [34] Ulrike Von Luxburg. A tutorial on spectral clustering. *Statistics and computing*, 17:395–416, 2007.
- [35] Jeffrey Wood and John Shawe-Taylor. Representation theory and invariant neural networks. *Discrete applied mathematics*, 69(1-2):33–60, 1996.

- [36] Keyulu Xu, Weihua Hu, Jure Leskovec, and Stefanie Jegelka. How powerful are graph neural networks? *International Conference on Learning Representations*, 2018.
- [37] Chulhee Yun, Suvrit Sra, and Ali Jadbabaie. Small relu networks are powerful memorizers: a tight analysis of memorization capacity. *Advances in Neural Information Processing Systems*, 32, 2019.
- [38] Manzil Zaheer, Satwik Kottur, Siamak Ravanbakhsh, Barnabas Poczos, Russ R Salakhutdinov, and Alexander J Smola. Deep sets. *Advances in neural information processing systems*, 30, 2017.
- [39] Bohang Zhang, Guhao Feng, Yiheng Du, Di He, and Liwei Wang. A complete expressiveness hierarchy for subgraph gnns via subgraph weisfeiler-lehman tests. *International Conference on Machine Learning*, 2023.
- [40] Muhan Zhang and Pan Li. Nested graph neural networks. In *Advances in Neural Information Processing Systems*, volume 34, 2021.
- [41] Lingxiao Zhao, Wei Jin, Leman Akoglu, and Neil Shah. From stars to subgraphs: Uplifting any GNN with local structure awareness. In *International Conference on Learning Representations*, 2022.

Appendix

The appendix is organized as follows:

- In Appendix A, we provide some basic definitions that will be used in later sections of the paper.
- In Appendix B we discuss some theoretical aspects of our model implementation, and its relation to Equation (2).
- In Appendix C we define four natural general node marking policies and analyze their theoretical effects on our model, as well as their relation to some node-based node marking policies. Finally, we provide a principled derivation of one of these policies using the natural symmetry of our base object.
- In Appendix D.1 we compare our model to node-based subgraph GNNs, which are the most widely used variant of subgraph GNNs. Additionally, we demonstrate that different choices of coarsening functions can recover various existing subgraph GNN designs.
- In Appendix D.2 we demonstrate how our model can leverage the information provided by the coarsening function in an effective way, comparing its expressivity to a natural baseline which also leverages the coarsening function. We show that for all coarsening functions, we are at least as expressive as the baseline and that for some coarsening functions, our model is strictly more expressive.
- In Appendix E we delve deeper into the characterization of all linear maps $L : \mathbb{R}^{\mathcal{P}([n]) \times [n]} \rightarrow \mathbb{R}^{\mathcal{P}([n]) \times [n]}$ that are equivariant to the action of the symmetric group.
- In Appendix F we provide experimental details to reproduce the results in Section 6, as well as a comprehensive set of ablation studies.
- In Appendix G we provide detailed proofs to all propositions in this paper.

A Basic Definitions

We devote this section to formally defining the key concepts of this paper, as well as introducing new useful notation. We start by defining the two principle components of our pipeline, the cartesian product graph and the coarsening function:

Definition A.1 (Cartesian Product Graph). *Given two graphs G_1 and G_2 , their Cartesian product $G_1 \square G_2$ is defined as:*

- The vertex set $V(G_1 \square G_2) = V(G_1) \times V(G_2)$.
- Vertices (u_1, u_2) and (v_1, v_2) in $G_1 \square G_2$ are adjacent if:
 - $u_1 = v_1$ and u_2 is adjacent to v_2 in G_2 , or
 - $u_2 = v_2$ and u_1 is adjacent to v_1 in G_1 .

Definition A.2 (Coarsening Function). *A Coarsening function $\mathcal{T}(\cdot)$ is defined as a function that, given a graph $G = (V, E)$ with vertex set $V = [n]$ and adjacency matrix $A \in \mathbb{R}^{n \times n}$, takes A as input and returns a set of "super-nodes" $\mathcal{T}(A) \subseteq \mathcal{P}([n])$. The function $\mathcal{T}(\cdot)$ is considered equivariant if, for any permutation $\sigma \in S_n$, the following condition holds:*

$$\mathcal{T}(\sigma \cdot A) = \sigma \cdot \mathcal{T}(A). \quad (11)$$

Here, $\sigma \cdot A$, and $\sigma \cdot \mathcal{T}(A)$ represent the group action of the symmetric group S_n on $\mathbb{R}^{n \times n}$, and $\mathcal{P}([n])$ respectively.

A coarsening function allows us to naturally define a graph structure on the "super-nodes" obtained from a given graph in the following way:

Definition A.3 (Coarsened Graph). *Given a coarsening function $\mathcal{T}(\cdot)$ and a graph $G = (V, E)$ with vertex set $V = [n]$, adjacency matrix $A \in \mathbb{R}^{n \times n}$, we abuse notation and define the coarsened graph $\mathcal{T}(G) = (V^\mathcal{T}, E^\mathcal{T})$ as follows:*

- $V^\mathcal{T} = \mathcal{T}(A)$

$$\bullet E^\mathcal{T} = \{\{S, S'\} \mid S, S' \in \mathcal{T}(A), \exists i \in S, i' \in S' \text{ s.t. } A_{i,i'} = 1\}.$$

The adjacency matrix of the coarsened graph can be expressed in two ways. The dense representation $A_{dense}^\mathcal{T} \in \mathbb{R}^{|V^\mathcal{T}| \times |V^\mathcal{T}|}$ is defined by:

$$A_{dense}^\mathcal{T}(S, S') = \begin{cases} 1 & \{S, S'\} \in E^\mathcal{T} \\ 0 & \text{otherwise.} \end{cases} \quad (12)$$

The sparse representation $A_{sparse}^\mathcal{T} \in \mathbb{R}^{\mathcal{P}([n]) \times \mathcal{P}([n])}$ is defined by:

$$A_{sparse}^\mathcal{T}(S, S') = \begin{cases} 1 & S, S' \in V^\mathcal{T}, \{S, S'\} \in E^\mathcal{T} \\ 0 & \text{otherwise.} \end{cases} \quad (13)$$

We note that if the coarsened graph $\mathcal{T}(G)$ has a corresponding node feature map $\mathcal{X} : V^\mathcal{T} \rightarrow \mathbb{R}^d$, it also has sparse and dense vector representations defined similarly. Though the dense representation seems more natural, the sparse representation is also useful, as the symmetric group S_n acts on it by:

$$\sigma \cdot A_{sparse}^\mathcal{T}(S, S') = A_{sparse}^\mathcal{T}(\sigma^{-1}(S), \sigma^{-1}(S')). \quad (14)$$

When the type of representation is clear from context, we abuse notation and write $A^\mathcal{T}$. Note also that in the above discussion, we have used the term "node feature map". Throughout this paper, in order to denote the node features of a graph $G = (V, E)$ with $|V| = n$, we use both the vector representation $X \in \mathbb{R}^{n \times d}$ and the map representation $\mathcal{X} : V \rightarrow \mathbb{R}^d$ interchangeably. Now, recalling that our pipeline is defined to create and update a node feature map $\mathcal{X}(S, v)$ supported on the nodes of the product graph $G \square \mathcal{T}(G)$, we define a general node marking policy, the following way:

Definition A.4 (General Node Marking Policy). *A general node marking policy $\pi(\cdot, \cdot)$, is a function which takes as input a graph $G = (V, E)$, and a coarsening function $\mathcal{T}(\cdot)$, and returns a node feature map $\mathcal{X} : V^\mathcal{T} \times V \rightarrow \mathbb{R}^d$.*

In Appendix C We provide four different node marking policies, and analyze the effect on our pipeline. We now move on to define the general way in which we update a given node feature map on the product graph.

Definition A.5 (General CS-GNNLayer Update). *Given a graph $G = (V, E)$ and a coarsening function $\mathcal{T}(\cdot)$, let $\mathcal{X}^t(S, v) : V \times V^\mathcal{T} \rightarrow \mathbb{R}^d$ denote the node feature map at layer t . The general CS-GNNlayer update is defined by:*

$$\begin{aligned} \mathcal{X}^{t+1}(S, v) = f^t \Big(& \mathcal{X}^t(S, v), \\ & \text{agg}_1^t \{ \{ \mathcal{X}^t(S, v'), e_{v,v'} \} \mid v' \sim_G v \}, \\ & \text{agg}_2^t \{ \{ \mathcal{X}^t(S', v), \tilde{e}_{S,S'} \} \mid S' \sim_{G^\mathcal{T}} S \}, \\ & \text{agg}_3^t \{ \{ \mathcal{X}^t(S', v), z(S, v, S', v) \} \mid S' \in V^\mathcal{T} \text{ s.t. } v \in S \}, \\ & \text{agg}_4^t \{ \{ \mathcal{X}^t(S, v'), z(S, v, S, v') \} \mid v' \in V \text{ s.t. } v' \in S \} \Big). \end{aligned} \quad (15)$$

Here, f^t is an arbitrary (parameterized) continuous function, agg_i^t , $i = 1, \dots, 4$ are learnable permutation invariant aggregation functions, $e_{v,v'}$, $\tilde{e}_{S,S'}$ are the (optional) edge features of G and $\mathcal{T}(G)$ respectively and the function $z : \mathcal{P}([n]) \times [n] \times \mathcal{P}([n]) \times [n] \rightarrow \mathbb{R}^d$ maps each tuple of indices $\mathbf{v} = (S, v, S', v')$ to a vector uniquely encoding the orbit of \mathbf{v} under the action of S_n as described in 72.

We note that for brevity, the notation used in the main body of the paper omits the aggregation functions $\text{agg}_1^t, \dots, \text{agg}_4^t$ and the edge features from the formulation of some of the layer updates. However, we explicitly state each component of the update, as we heavily utilize them in later proofs. We also note that this update is different than the general layer update presented in Equation (2), as it doesn't use all global updates characterized in 9. The reason for this is that some of the global updates have an asymptotic runtime of $\tilde{O}(n^2)$ where n is the number of nodes in the input graph. As our goal was to create models that improve on the scalability of standard subgraph GNNs which have

an asymptotic runtime of $\tilde{O}(n^2)$. We decided to discard some of the general global updates and keep only the ones that are induced by the last two entries in equation 15 which all have a linear runtime. After a stacking of the layers in Equation (15), we employ the following pooling procedure on the final node feature map \mathcal{X}^T :

$$\rho(\mathcal{X}^T) = \text{MLP}_2 \left(\sum_{S \in V^\tau} \left(\text{MLP}_1 \left(\sum_{v \in V} \mathcal{X}^T(S, v) \right) \right) \right). \quad (16)$$

Finally, we define the set of all functions that can be expressed by our model:

Definition A.6 (Expressivity of Family of Graph Functions). *Let \mathcal{F} be a family of graph functions, we say that \mathcal{F} can express a graph function $g(\cdot)$ if for every finite family of graphs \mathcal{G} there exists a function $f \in \mathcal{F}$ such that:*

$$f(G) = g(G) \quad \forall G \in \mathcal{G}. \quad (17)$$

Here, \mathcal{G} is a finite family of graphs if all possible values of node/edge features of the graphs in \mathcal{G} form a finite set, and the maximal size of the graphs within \mathcal{G} is bounded.

Definition A.7 (Family of Functions Expressed By CS-GNN). *Let π be a general node marking policy and \mathcal{T} be a coarsening function. Define $\mathcal{S}(\mathcal{T}, \pi)$ to be the family of graph functions, which when given input graph $G = (V, E)$, first compute $\mathcal{X}^0(S, v)$ using $\pi(G, \mathcal{T})$, then update this node feature map by stacking T layers of the form 15, and finally pooling $\mathcal{X}^0(S, v)$ using equation 16. We define $\text{CS-GNN}(\mathcal{T}, \pi)$ to be the set of all functions that can be expressed by $\mathcal{S}(\mathcal{T}, \pi)$.*

B Theoretical Validation of Implementation Details

In this section, we provide implementation details of our model and prove that they enable us to recover the conceptual framework of the model discussed thus far. First, we note that in Section 4.2, we characterized all equivariant linear maps $L : \mathbb{R}^{\mathcal{P}([n]) \times [n]} \rightarrow \mathbb{R}^{\mathcal{P}([n]) \times [n]}$ in order to incorporate them into our layer update. Given the high dimensionality of the space of all such linear maps, and in order to save parameters, we demonstrate that it is possible to integrate these layers into our layer update by adding edge features to a standard MPNN model. This is formalized in the following proposition:

Lemma B.1 (Parameter Sharing as MPNN). *Let $B_1, \dots, B_k : \mathbb{R}^{n \times n}$ be orthogonal matrices with entries restricted to 0 or 1, and let $W_1, \dots, W_k \in \mathbb{R}^{d \times d'}$ denote a sequence of weight matrices. Define $B_+ = \sum_{i=1}^k B_i$ and choose $z_1, \dots, z_k \in \mathbb{R}^{d^*}$ to be a set of unique vectors representing an encoding of the index set. The function that represents an update via parameter sharing:*

$$f(X) = \sum_{i=1}^k B_i X W_i, \quad (18)$$

can be implemented on any finite family of graphs \mathcal{G} , by a stack of MPNN layers of the following form [13],

$$m_v^l = \sum_{u \in N_{B_+}(v)} M^l(X_u^l, e_{u,v}), \quad (19)$$

$$X_v^{l+1} = U^l(X_v^l, m_v^l), \quad (20)$$

where U^l, M^l are multilayer perceptrons (MLPs). The inputs to this MPNN are the adjacency matrix B_+ , node feature vector X , and edge features – the feature of edge (u, v) is given by:

$$e_{u,v} = \sum_{i=1}^k z_i \cdot B_i(u, v). \quad (21)$$

Here, $B_i(u, v)$ denotes the (u, v) entry to matrix B_i .

The proof is given in Appendix G. The analysis in Section 4.2 demonstrates that the basis of the space of all equivariant linear maps $L : \mathbb{R}^{\mathcal{P}([n]) \times [n]} \rightarrow \mathbb{R}^{\mathcal{P}([n]) \times [n]}$ satisfies the conditions of Lemma F.1. Additionally, we notice that some of the equivariant linear functions have an asymptotic runtime of

$\tilde{O}(n^2)$ where n is the number of nodes in the input graph. As our main goal is to construct a more scalable alternative to node-based subgraph GNNs, which also have a runtime of $\tilde{O}(n^2)$, we limit ourselves to a subset of the basis for which all maps run in linear time. This is implemented by adding edge features to the adjacency matrices A_{P_1} and A_{P_2} , defined later in this section.

We now move on to discussing our specific implementation of the general layer update from Definition A.5.

Given a graph $G = (V, E)$ and a coarsening function \mathcal{T} , we aim to implement this general layer update by combining several standard message passing updates on the product graph $G \square \mathcal{T}(G)$. In the next two definitions, we define the adjacency matrices supported on the node set $V \times V^{\mathcal{T}}$, which serve as the foundation for these message passing procedures, and formalize the procedures themselves.

Definition B.1 (Adjacency Matrices on Product Graph). *Let $G = (V, E)$ be a graph with adjacency matrix A and node feature vector X , and let $\mathcal{T}(\cdot)$ be a coarsening function. We define the following four adjacency matrices on the vertex set $V^{\mathcal{T}} \times V$:*

$$A_G(S, v, S', v') = \begin{cases} 1 & v \sim_G v', S = S' \\ 0 & \text{otherwise.} \end{cases} \quad (22)$$

$$A_{\mathcal{T}(G)}(S, v, S', v') = \begin{cases} 1 & S \sim_{\mathcal{T}(G)} S', v = v' \\ 0 & \text{otherwise.} \end{cases} \quad (23)$$

$$A_{P_1}(S, v, S', v') = \begin{cases} 1 & v \in S', v = v' \\ 0 & \text{otherwise.} \end{cases} \quad (24)$$

$$A_{P_2}(S, v, S', v') = \begin{cases} 1 & v' \in S, S' = S \\ 0 & \text{otherwise.} \end{cases} \quad (25)$$

Given edge features $\{e_{v,v'} \mid v \sim_G v'\}$ and $\{\tilde{e}_{S,S'} \mid S \sim_{\mathcal{T}(G)} S'\}$ corresponding to the graphs G and $\mathcal{T}(G)$, respectively, we can trivially define the edge features corresponding to A_G and $A_{G\mathcal{T}}$ as follows:

$$e_G(S, v, S', v') = e_{v,v'}, \quad (26)$$

$$e_{\mathcal{T}(G)}(S, v, S', v') = \tilde{e}_{S,S'}. \quad (27)$$

In addition, for $i = 1, 2$, we define the edge features corresponding to adjacency matrices A_{P_i} as follows:

$$e_{P_i}(S, v, S', v') = z(S, v, S', v'). \quad (28)$$

Here, the function $z : \mathcal{P}([n]) \times [n] \times \mathcal{P}([n]) \times [n] \rightarrow \mathbb{R}^d$ maps each tuple $\mathbf{v} = (S, v, S', v')$ to a vector uniquely encoding the orbit of \mathbf{v} under the action of S_n as described in Equation 72.

Definition B.2 (CS-GNN Update Implementation). *Given a graph $G = (V, E)$, and a coarsening function $\mathcal{T}(\cdot)$, let $A_1 \dots A_4$ enumerate the set of adjacency matrices $\{A_G, A_{\mathcal{T}(G)}, A_{P_1}, A_{P_2}\}$. We define a CS-GNN layer update in the following way:*

$$\mathcal{X}_i^t(S, v) = U_i^t \left((1 + \epsilon_i^t) \cdot \mathcal{X}^t(S, v) + \sum_{(S', v') \sim_{A_i}(S, v)} M^t(\mathcal{X}^t(S', v') + e_i(S, v, S', v')) \right). \quad (29)$$

$$\mathcal{X}^{t+1}(S, v) = U_{fin}^t \left(\sum_{i=1}^4 \mathcal{X}_i^t(S, v) \right). \quad (30)$$

Here $\mathcal{X}^t(S, v)$ and $\mathcal{X}^{t+1}(S, v)$ denote the node feature maps of the product graph at layers t and $t + 1$, respectively. $e^1(S, v, S', v'), \dots, e^4(S, v, S', v')$ denote the edge features associated with adjacency matrices A_1, \dots, A_4 . $\epsilon_1^t, \dots, \epsilon_4^t$ represent learnable parameters in \mathbb{R} , and $U_1^t, \dots, U_4^t, U_{fin}^t$, M^t all refer to multilayer perceptrons.

The next proposition states that using the layer update defined in equations 29 and 30 is enough to efficiently recover the general layer update defined in equation 15.

Proposition B.1 (Equivalence of General Layer and Implemented Layer). *Let $\mathcal{T}(\cdot)$ be a coarsening function, π be a generalized node marking policy, and \mathcal{G} be a finite family of graphs. Applying a stack of t general layer updates as defined in Equation 15 to the node feature map $\mathcal{X}(S, v)$ induced by $\pi(G, \mathcal{T})$, can be effectively implemented by applying a stack of t layer updates specified in Equations 29 and 30 to $\mathcal{X}(S, v)$. Additionally, the depths of all MLPs that appear in 29 and 30 can be bounded by 4.*

C Node Marking Policies – Theoretical Analysis

In this section, we define and analyze various general node marking policies, starting with four natural choices.

Definition C.1 (Four General Node Marking policies). *Let $G = (V, E)$ be a graph with adjacency matrix $A \in \mathbb{R}^{n \times n}$ and node feature vector $X \in \mathbb{R}^{n \times d}$, and let $\mathcal{T}(\cdot)$ be a coarsening function. All of the following node marking policies take the form:*

$$\pi(G, \mathcal{T}) = \mathcal{X}(S, v) = [X_u, b_\pi(S, v)], \quad (31)$$

where $[\cdot, \cdot]$ denotes the concatenation operator. We focus on four choices for $b_\pi(S, v)$:

1. Simple Node Marking:

$$b_\pi(S, v) = \begin{cases} 1 & \text{if } v \in S, \\ 0 & \text{if } v \notin S. \end{cases} \quad (32)$$

We denote this node marking policy by π_S .

2. Node + Size Marking:

$$b_\pi(S, v) = \begin{cases} (1, |S|) & \text{if } v \in S, \\ (0, |S|) & \text{if } v \notin S. \end{cases} \quad (33)$$

We denote this node marking policy by π_{SS} .

3. Minimum Distance:

$$b_\pi(S, v) = \min_{v' \in S} d_G(v, v') \quad (34)$$

where $d_G(v, v')$ is the shortest path distance between nodes v and v' in the original graph. We denote this node marking policy by π_{MD} .

4. Learned Distance Function:

$$b_\pi(S, v) = \phi(\{d_G(v, v') \mid v' \in S\}) \quad (35)$$

where $\phi(\cdot)$ is a learned permutation-invariant function. We denote this node marking policy by π_{LD} .

We note that when using the identity coarsening function $\mathcal{T}(G) = G$, our general node marking policies output node feature maps supported on the product $V \times V$. Thus, they can be compared to node marking policies used in node-based subgraph GNNs. In fact, in this case, both π_S and π_{SS} reduce to classical node-based node marking, while π_{MD} and π_{LD} reduce to distance encoding. The definitions of these can be found in [39]. Interestingly, even though in the case of node-based subgraph GNNs, both distance encoding and node marking were proven to be maximally expressive [39], in our case for some choices of \mathcal{T} , π_{LD} is strictly more expressive than the other three choices. The exact effect of each generalized node marking policy on the expressivity of our model is explored in the following two propositions.

Proposition C.1 (Equal Expressivity of Node Marking Policies). *For any coarsening function $\mathcal{T}(\cdot)$ the following holds:*

$$CS\text{-}GNN(\mathcal{T}, \pi_S) = CS\text{-}GNN(\mathcal{T}, \pi_{SS}) = CS\text{-}GNN(\mathcal{T}, \pi_{MD}). \quad (36)$$

Proposition C.2 (Expressivity of Learned Distance Policy). *For any coarsening function $\mathcal{T}(\cdot)$ the following holds:*

$$CS\text{-}GNN(\mathcal{T}, \pi_S) \subseteq CS\text{-}GNN(\mathcal{T}, \pi_{LD}). \quad (37)$$

In addition, for some choices of $\mathcal{T}(\cdot)$ the containment is strict.

The proofs of both propositions can be found in Appendix G. Finally, we provide a principled approach to deriving a generalized node marking policy based on symmetry invariance, and prove its equivalence to π_{SS} . Given a graph $G = (V, E)$ with $V = [n]$, adjacency matrix A , and node feature vector $X \in \mathbb{R}^{n \times d}$, along with a coarsening function $\mathcal{T}(\cdot)$, We define an action of the symmetric group S_n on the space $\mathbb{R}^{\mathcal{P}([n]) \times [n]}$ as follows:

$$\sigma \cdot \mathcal{X}(S, v) = \mathcal{X}(\sigma^{-1}(S), \sigma^{-1}(v)) \quad \text{for } \sigma \in S_n, \mathcal{X} \in \mathbb{R}^{\mathcal{P}([n]) \times [n]}. \quad (38)$$

Now, for each orbit $\gamma \in (\mathcal{P}([n]) \times [n]) / S_n$, we define $\mathbf{1}_\gamma \in \mathbb{R}^{\mathcal{P}([n]) \times [n]}$ as follows:

$$\mathbf{1}_\gamma(S, v) = \begin{cases} 1 & (S, v) \in \gamma, \\ 0 & \text{otherwise.} \end{cases} \quad (39)$$

Choosing some enumeration of the orbit set $(\mathcal{P}([n]) \times [n]) / S_n = \{\gamma_1, \dots, \gamma_k\}$, We now define the invariant generalized node marking policy π_{inv} by first setting:

$$b_{\pi_{\text{inv}}}^{\text{sparse}}(S, v) : \mathcal{P}([n]) \times [n] \rightarrow \mathbb{R}^k$$

and

$$b_{\pi_{\text{inv}}} : V^{\mathcal{T}} \times V \rightarrow \mathbb{R}^k$$

as follows:

$$b_{\pi_{\text{inv}}}^{\text{sparse}}(S, v) = [\mathbf{1}_{\gamma_1}(S, v), \dots, \mathbf{1}_{\gamma_k}(S, v)] \quad S \in \mathcal{P}(V), v \in V, \quad (40)$$

$$b_{\pi_{\text{inv}}}(S, v) = b_{\pi_{\text{inv}}}^{\text{sparse}}(S, v) \quad S \in V^{\mathcal{T}}, v \in V. \quad (41)$$

Then, we define the node feature map induced by π_{inv} as:

$$\mathcal{X}^{\pi_{\text{inv}}}(S, v) = [X_v, b_{\pi_{\text{inv}}}(S, v)]. \quad (42)$$

Interestingly, π_{inv} , derived solely from the group action of S_n on $\mathcal{P}([n]) \times [n]$, is equivalent to the generalized node marking policy π_{SS} . This is stated more rigorously in the following proposition:

Proposition C.3 (Node + Size Marking as Invariant Marking). *Given a graph $G = (V, E)$ with node feature vector $X \in \mathbb{R}^{n \times d}$, and a coarsening function $\mathcal{T}(\cdot)$, let $\mathcal{X}^{\pi_{SS}}, \mathcal{X}^{\pi_{\text{inv}}}$ be the node feature maps induced by π_{SS} and π_{inv} respectively. Recall that:*

$$\mathcal{X}^{\pi_{SS}}(S, v) = [X_v, b_{\pi_{SS}}(S, v)], \quad (43)$$

$$\mathcal{X}^{\pi_{\text{inv}}}(S, v) = [X_v, b_{\pi_{\text{inv}}}(S, v)]. \quad (44)$$

The following now holds:

$$b_{\pi_{\text{inv}}}(S, v) = \text{OHE}(b_{\pi_{SS}}(S, v)) \quad \forall S \in V^{\mathcal{T}}, \forall v \in V. \quad (45)$$

Here, OHE denotes a one-hot encoder, independent of the choice of both G and \mathcal{T} .

The proof of proposition C.3 can be found in Appendix G.

D Expressive Power of CS-GNN

D.1 Recovering Subgraph GNNs

In this section, we demonstrate that by choosing suitable coarsening functions, our architecture can replicate various previous subgraph GNN designs. We begin by focusing on node-based models, which are the most widely used type. We define a variant of these models which was proven in [39] to be maximally expressive, and show that our approach can recover it.

Definition D.1 (Maximally Expressive Subgraph GNN). *We define $MSGNN(\pi_{NM})$ as the set of all functions expressible by the following procedure:*

1. **Node Marking:** The representation of tuple $(u, v) \in V \times V$ is initially given by:

$$\mathcal{X}^0(u, v) = \begin{cases} 1 & \text{if } u = v, \\ 0 & \text{if } u \neq v. \end{cases} \quad (46)$$

2. **Update:** The representation of tuple (u, v) is updated according to:

$$\begin{aligned} \mathcal{X}^{t+1}(u, v) = f^t & \left(\mathcal{X}^t(u, v), \mathcal{X}^t(u, u), \mathcal{X}^t(v, v), \right. \\ & \text{agg}_1^t \{ \{ \mathcal{X}^t(u, v'), e_{v, v'} \} \mid v' \sim v \}, \\ & \left. \text{agg}_2^t \{ \{ \mathcal{X}^t(v, u'), e_{u, u'} \} \mid u' \sim u \} \right). \end{aligned} \quad (47)$$

3. **Pooling:** The final node feature vector $\mathcal{X}^T(u, v)$ is pooled according to:

$$\text{MLP}_2 \left(\sum_{u \in V} \text{MLP}_1 \left(\sum_{v \in V} \mathcal{X}^T(u, v) \right) \right). \quad (48)$$

Here, for any $t \in [T]$, f^t is any continuous (parameterized) functions, $\text{agg}_1^t, \text{agg}_2^t$ are any continuous (parameterized) permutation-invariant functions and $\text{MLP}_1, \text{MLP}_2$ are multilayer perceptrons.

Proposition D.1 (CS-GNN Can Implement MSGNN). *Let $\mathcal{T}(\cdot)$ be the identity coarsening function defined by:*

$$\mathcal{T}(G) = \{ \{v\} \mid v \in V \} \quad \forall G = (V, E). \quad (49)$$

The following holds:

$$\text{CS-GNN}(\mathcal{T}, \pi_S) = \text{MSGNN}(\pi_{NM}). \quad (50)$$

The proof of proposition D.1 can be found in Appendix G. We observe that, similarly, by selecting the coarsening function:

$$\mathcal{T}(G) = E \quad \forall G = (V, E), \quad (51)$$

one can recover edge-based subgraph GNNs. An example of such a model is presented in [4] (DS-GNN), where it was proven capable of distinguishing between two 3-WL indistinguishable graphs, despite having an asymptotic runtime of $\tilde{O}(m^2)$, where m is the number of edges in the input graph. This demonstrates our model’s ability to achieve expressivity improvements while maintaining a (relatively) low asymptotic runtime by exploiting the graph’s sparsity through the coarsening function. Finally, we note that by selecting the coarsening function:

$$\mathcal{T}(G) = \{ S \in \mathcal{P}(V) \mid |S| = k \} \quad G = (V, E), \quad (52)$$

We can recover an unordered variant of the k -OSAN model presented in [30].

D.2 Comparison to Theoretical Baseline

In this section, we demonstrate how our model can leverage the information provided by the coarsening function $\mathcal{T}(\cdot)$ in an effective way. First, we define a baseline model that incorporates \mathcal{T} in a straightforward manner. We then prove that, for any $\mathcal{T}(\cdot)$, our model is at least as expressive as this baseline. Additionally, we show that for certain choices of $\mathcal{T}(\cdot)$, our model exhibits strictly greater expressivity. To construct the baseline model, we first provide the following definition:

Definition D.2 (Coarsened Sum Graph). *Given a graph $G = (V, E)$ and a coarsening function $\mathcal{T}(\cdot)$, we define the coarsened sum graph $G_+^T = (V_+^T, E_+^T)$ by:*

- $V_+^T = V \cup V^T$.
- $E_+^T = E \cup E^T \cup \{ \{S, v\} \mid S \in V^T, v \in V, v \in S \}$.

If graph G had a node feature vector $X \in \mathbb{R}^{n \times d}$, we define the node feature vector of G_+^T as:

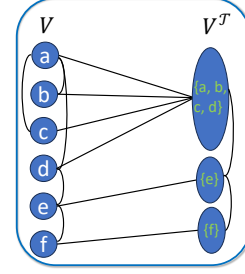
$$X_v = \begin{cases} [X_v, 1] & v \in V \\ 0_{d+1} & v \in V^T \end{cases}. \quad (53)$$

Here we concatenated a 1 to the end of node features of V to distinguish them from the nodes of V^T .

The connectivity of the sum graph (for our running example Figure 1) is visualized inset.

We now define our baseline model:

Definition D.3 (Coarse MPNN). *Let $\mathcal{T}(\cdot)$ be a coarsening function. Define $MPNN_+(\mathcal{T})$ as the set of all functions which can be expressed by the following procedure:*



1. **Preprocessing:** We first construct the sum graph G_+^T of the input graph G , along with a node feature map $\mathcal{X}^0 : V_+^T \rightarrow \mathbb{R}^d$ defined according to equation 53.
2. **Update:** The representation of node $v \in V_+^T$ is updated according to:

$$\begin{aligned}
 \text{For } v \in V : \quad \mathcal{X}^{t+1}(v) &= f_V^t(\mathcal{X}^t(v), \text{agg}_1^t\{\{\mathcal{X}^t(u), e_{u,v} \mid u \sim_G v\}\}, \\
 &\quad \text{agg}_2^t\{\{\mathcal{X}^t(S) \mid S \in V^T, v \in S\}\}), \\
 \text{For } S \in V^T : \quad \mathcal{X}^{t+1}(S) &= f_{V^T}^t(\mathcal{X}^t(S), \text{agg}_1^t\{\{\mathcal{X}^t(S'), e_{S,S'} \mid S' \sim_{\mathcal{T}(G)} S\}\}, \\
 &\quad \text{agg}_2^t\{\{\mathcal{X}^t(v) \mid v \in V, v \in S\}\}).
 \end{aligned} \tag{54}$$

3. **Pooling:** The final node feature vector $\mathcal{X}^T(\cdot)$ is pooled according to:

$$MLP\left(\sum_{v \in V_+^T} \mathcal{X}^T(v)\right). \tag{55}$$

Here, for $t \in [T]$, $f_V^t, f_{V^T}^t$ are continuous (parameterized) functions and $\text{agg}_1^t, \text{agg}_2^t$ are continuous (parameterized) permutation invariant functions. Finally, we notice that for the trivial coarsening function defined by

$$\mathcal{T}_\emptyset(G) = \emptyset, \tag{56}$$

the update in Equation (54) devolves into a standard MPNN update, as defined in [13] and so we define:

$$MPNN = MPNN_+(\mathcal{T}_\emptyset). \tag{57}$$

In essence, given an input graph $G = (V, E)$, the $MPNN_+(\mathcal{T})$ pipeline first constructs the coarsened graph $\mathcal{T}(G)$. It then adds edges between each super-node $S \in V^T$ and the nodes it is comprised of (i.e., any $v \in S$). This is followed by a standard message passing procedure on the graph. The following two propositions suggest that this simple approach to incorporating \mathcal{T} into a GNN pipeline is less powerful than our model.

Proposition D.2 (CS-GNN Is at Least as Expressive as Coarse MPNN). *For any coarsening function $\mathcal{T}(\cdot)$ the following holds:*

$$MPNN \subseteq MPNN_+(\mathcal{T}) \subseteq CS\text{-}GNN(\mathcal{T}, \pi_S) \tag{58}$$

Proposition D.3 (CS-GNN Can Be More Expressive Than $MPNN_+$). *Let $\mathcal{T}(\cdot)$ be the identity coarsening function defined by:*

$$\mathcal{T}(G) = \{\{v\} \mid v \in V\} \quad G = (V, E). \tag{59}$$

The following holds:

$$MPNN = MPNN_+(\mathcal{T}). \tag{60}$$

Thus:

$$MPNN_+(\mathcal{T}) \subset CS\text{-}GNN(\mathcal{T}, \pi_S), \tag{61}$$

where this containment is strict.

The proofs to the last two propositions can be found in Appendix G. Proposition D.3 demonstrates that CS-GNNs are strictly more expressive than MPNN_+ when using the identity coarsening function. However, this result extends to more complex coarsening functions as well. We briefly discuss one such example. Let $\mathcal{T}(\cdot)$ be the coarsening function defined by:

$$\mathcal{T}_\Delta(G) = \{v_1, v_2, v_3 \mid G[v_1, v_2, v_3] \cong \Delta\}, \quad (62)$$

i.e. for an input graph G , the set of super-nodes is composed of all triplets of nodes whose induced subgraph is isomorphic to a triangle. To see that CS-GNN is strictly more expressive than MPNN_+ when using $\mathcal{T}_\Delta(\cdot)$, we look at the two graphs G and H depicted in Figure 4. In the figure, we see the two original graphs, G and H , their corresponding sum graphs $G_+^{\mathcal{T}_\Delta}$ and $H_+^{\mathcal{T}_\Delta}$, and a subgraph of their corresponding product graphs $G \square \mathcal{T}_\Delta(G)$ and $H \square \mathcal{T}_\Delta(H)$ induced by the sets $\{(S_0, v) \mid v \in V_G\}$ and $\{(S_0, v) \mid v \in V_H\}$ respectively (this can be thought of as looking at a single subgraph from the bag of subgraphs induced by CS-GNN). One can clearly see that both the original graphs and their respective sum graphs are 1-WL indistinguishable. On the other hand, the subgraphs induced by our method are 1-WL distinguishable. Since for both G and H the "bag of subgraphs" induced by CS-GNN is composed of 6 isomorphic copies of the same graph, this would imply that our method can distinguish between G and H , making it strictly more expressive than MPNN_+ .

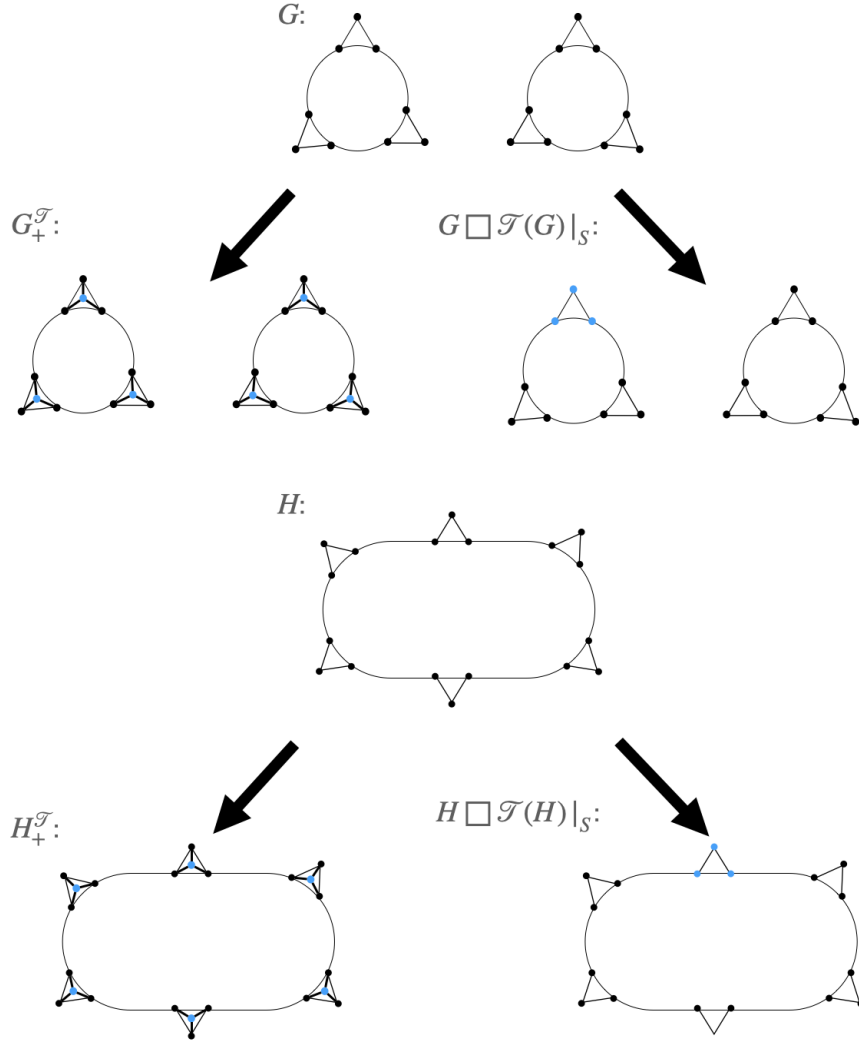


Figure 4: Rows 1 and 3 depict two 1-WL indistinguishable graphs. Rows 2 and 4 depict the sum graph of each of these graphs, as well as one subgraph of their product graphs induced by all node, super-node tuples whose super-node is fixed.

E Linear Invariant (Equivariant) Layer – Extended Section

We introduce some key notation. In the matrix \mathcal{X} , the i -th row corresponds to the i -th subset S arranged in the lexicographic order of all subsets of $[n]$, namely, $\{\{0\}, \{0, 1\}, \{0, 2\}, \dots, \{0, 1, 2, \dots, n\}\}$. Each i -th position in this sequence aligns with the i -th row index in \mathcal{X} . It follows, that the standard basis for such matrices in $\mathbb{R}^{2^n \times n}$ is expressed as $\mathbf{e}^{(S)} \cdot \mathbf{e}^{(i)^T}$, where $\mathbf{e}^{(S)}$ is a 1-hot vector, with the value 1 positioned according to S in the lexicographic order. For a matrix $X \in \mathbb{R}^{a \times b}$, the operation of vectorization, denoted by $\text{vec}(X)$, transforms X into a single column vector in $\mathbb{R}^{ab \times 1}$ by sequentially stacking its columns; in the context of \mathcal{X} , the basis vectors of those vectors are $\mathbf{e}^{(i)} \otimes \mathbf{e}^{(S)}$. The inverse process, reshaping a vectorized matrix back to its original format, is denoted as $[\text{vec}(X)] = X$. We also denote an arbitrary permutation by $\sigma \in S_n$. The actions of permutations on vectors, whether indexed by sets or individual indices, are represented by $\mathbf{P}_S \in \text{GL}(2^n)$ and $\mathbf{P}_I \in \text{GL}(n)$, respectively. This framework acknowledges S_n as a subgroup of the larger permutation group S_{2^n} , which permutes all 2^n positions in a given vector $\mathbf{v}_S \in \mathbb{R}^{2^n}$.

Let $\mathbf{L} \in \mathbb{R}^{1 \times 2^n \cdot n}$ be the matrix representation of a general linear operator $\mathcal{L} : \mathbb{R}^{2^n \times n} \rightarrow \mathbb{R}$ in the standard basis. The operator \mathcal{L} is order-invariant iff

$$\mathbf{L} \text{vec}(\mathbf{P}_S^T \mathcal{X} \mathbf{P}_I) = \mathbf{L} \text{vec}(\mathcal{X}). \quad (63)$$

Similarly, let $\mathbf{L} \in \mathbb{R}^{2^n \cdot n \times 2^n \cdot n}$ denote the matrix for $\mathcal{L} : \mathbb{R}^{2^n \times n} \rightarrow \mathbb{R}^{2^n \times n}$. The operator \mathcal{L} is order-equivariant if and only if

$$[\mathbf{L} \text{vec}(\mathbf{P}_S^T \mathcal{X} \mathbf{P}_I)] = \mathbf{P}_S^T [\mathbf{L} \text{vec}(\mathcal{X})] \mathbf{P}_I. \quad (64)$$

Using properties of the Kronecker product (see Appendices E.1 and E.2 for details), we derive the following conditions for invariant and equivariant linear layers:

$$\text{Invariant } \mathbf{L} : \quad \mathbf{P}_I \otimes \mathbf{P}_S \text{vec}(\mathbf{L}) = \text{vec}(\mathbf{L}), \quad (65)$$

$$\text{Equivariant } \mathbf{L} : \quad \mathbf{P}_I \otimes \mathbf{P}_S \otimes \mathbf{P}_I \otimes \mathbf{P}_S \text{vec}(\mathbf{L}) = \text{vec}(\mathbf{L}). \quad (66)$$

Solving Equations (65) and (66). Let $\sigma \in S_n$ denote a permutation corresponding to the permutation matrix \mathbf{P} . Let $\mathbf{P} \star \mathbf{L}$ denote the tensor that results from expressing \mathbf{L} after renumbering the nodes in V^T, V according to the permutation σ . Explicitly, for $\mathbf{L} \in \mathbb{R}^{2^n \times n}$, the $(\sigma(S), \sigma(i))$ -entry of $\mathbf{P} \star \mathbf{L}$ equals to the (S, i) -entry of \mathbf{L} . The matrix that corresponds to the operator $\mathbf{P} \star$ in the standard basis, $\mathbf{e}^{(i)} \otimes \mathbf{e}^{(S)}$ is the kronecker product $\mathbf{P}_I \otimes \mathbf{P}_S$. Since $\text{vec}(\mathbf{L})$ is exactly the coordinate vector of the tensor \mathbf{L} in the standard basis we have,

$$\text{vec}(\mathbf{P} \star \mathbf{L}) = \mathbf{P}_I \otimes \mathbf{P}_S \text{vec}(\mathbf{L}), \quad (67)$$

following the same logic, the following holds for the equivariant case, where $\mathbf{L} \in \mathbb{R}^{2^n \cdot n \times 2^n \cdot n}$,

$$\text{vec}(\mathbf{P} \star \mathbf{L}) = \mathbf{P}_I \otimes \mathbf{P}_S \otimes \mathbf{P}_I \otimes \mathbf{P}_S \text{vec}(\mathbf{L}). \quad (68)$$

Given Equations (65) and (67) and Equations (66) and (68), it holds that we should focus on solving,

$$\mathbf{P} \star \mathbf{L} = \mathbf{L}, \quad \forall \mathbf{P} \text{ permutation matrices}, \quad (69)$$

for both cases where $\mathbf{L} \in \mathbb{R}^{2^n \times n}$ and $\mathbf{L} \in \mathbb{R}^{2^n \cdot n \times 2^n \cdot n}$, corresponding to the bias term, and linear term.

Bias. To this end, let us define an equivalence relation in the index space of a tensor in $\mathbb{R}^{2^n \times n}$. Given a pair $(S, i) \in \mathcal{P}([n]) \times [n]$, we define γ^{k+} to correspond to all pairs (S, i) such that $|S| = k$ and $i \notin S$. Similarly, γ^{k-} corresponds to all pairs (S, i) such that $|S| = k$ and $i \in S$. We denote this equivalence relation as follows:

$$(\mathcal{P}([n]) \times [n]) / \sim \triangleq \{\gamma^{k*} : k = 1, \dots, n; * \in \{+, -\}\}. \quad (70)$$

For each set-equivalence class $\gamma \in (\mathcal{P}([n]) \times [n]) / \sim$, we define a basis tensor, $\mathbf{B}^\gamma \in \mathbb{R}^{2^n \times n}$ by setting:

$$\mathbf{B}_{S,i}^\gamma = \begin{cases} 1, & \text{if } (S, i) \in \gamma; \\ 0, & \text{otherwise.} \end{cases} \quad (71)$$

Following similar reasoning, consider elements $(S_1, i_1, S_2, i_2) \in (\mathcal{P}([n]) \times [n] \times \mathcal{P}([n]) \times [n])$. We define a partition according to six conditions: the relationship between i_1 and i_2 , denoted as $i_1 \leftrightarrow i_2$, which is determined by the condition: $i_1 = i_2$ or $i_1 \neq i_2$; the cardinalities of S_1 and S_2 , denoted as k_1 and k_2 , respectively; the size of the intersection $S_1 \cap S_2$, denoted as k^\cap ; the membership of i_l in S_l for $l \in \{1, 2\}$, denoted as $\delta_{\text{same}} \in \{1, 2, 3, 4\}$; and the membership of i_{l_1} in S_{l_2} for distinct $l_1, l_2 \in \{1, 2\}$, denoted as $\delta_{\text{diff}} \in \{1, 2, 3, 4\}$. The equivalence relation thus defined can be represented as:

$$(\mathcal{P}([n]) \times [n] \times \mathcal{P}([n]) \times [n]) / \sim \triangleq \{\Gamma^{\leftrightarrow}; k_1; k_2; k^\cap; \delta_{\text{same}}; \delta_{\text{diff}}\}. \quad (72)$$

For each set-equivalence class $\Gamma \in (\mathcal{P}([n]) \times [n] \times \mathcal{P}([n]) \times [n]) / \sim$, we define a basis tensor, $\mathbf{B}^\Gamma \in \mathbb{R}^{2^n \times n \times 2^n \times n}$ by setting:

$$\mathbf{B}_{S_1, i_1; S_2, i_2}^\Gamma = \begin{cases} 1, & \text{if } (S_1, i_1, S_2, i_2) \in \Gamma; \\ 0, & \text{otherwise.} \end{cases} \quad (73)$$

The following two proposition summarizes the results in this section,

Lemma E.1 ($\gamma(\Gamma)$ are orbits). *The sets $\{\gamma^{k^*} : k = 1, \dots, n; * \in \{+, -\}\}$ and $\{\Gamma^{\leftrightarrow}; k_1; k_2; k^\cap; \delta_{\text{same}}; \delta_{\text{diff}}\}$ are the orbits of S_n on the index space $(\mathcal{P}([n]) \times [n])$ and $(\mathcal{P}([n]) \times [n] \times (\mathcal{P}([n]) \times [n]))$, respectively.*

Proposition E.1 (Basis of Invariant (Equivariant) Layer). *The tensors \mathbf{B}^γ (\mathbf{B}^Γ) in Equation (71) (Equation (73)) form an orthogonal basis (in the standard inner product) to the solution of Equation (65) (Equation (66)).*

The proofs are given in Appendix G.

E.1 Full Derivation of Equation (65).

Our goal is to transition from the equation,

$$\mathbf{L} \text{vec}(\mathbf{P}_S^T \mathcal{X} \mathbf{P}_T) = \mathbf{L} \text{vec}(\mathcal{X}) \quad (63)$$

to the form,

$$\mathbf{P}_T \otimes \mathbf{P}_S \text{vec}(\mathbf{L}) = \text{vec}(\mathbf{L}) \quad (65)$$

We introduce the following property of the Kronecker product,

$$\text{vec}(\mathbf{ABC}) = (\mathbf{C}^T \otimes \mathbf{A}) \text{vec}(\mathbf{B}). \quad (74)$$

Using Equation (74) on the left side of Equation (63), we obtain

$$\mathbf{L} \mathbf{P}_T^T \otimes \mathbf{P}_S^T \text{vec}(\mathcal{X}) = \mathbf{L} \text{vec}(\mathcal{X}), \quad (75)$$

since this should be true for any $\mathcal{X} \in \mathbb{R}^{2^n \times n}$, we derive

$$\mathbf{L} \mathbf{P}_T^T \otimes \mathbf{P}_S^T = \mathbf{L}. \quad (76)$$

Applying the transpose operation on both sides, and noting that $(\mathbf{P}_T^T \otimes \mathbf{P}_S^T)^T = \mathbf{P}_T \otimes \mathbf{P}_S$, we obtain

$$\mathbf{P}_T \otimes \mathbf{P}_S \mathbf{L}^T = \mathbf{L}^T. \quad (77)$$

Recalling that $\mathbf{L} \in \mathbb{R}^{1 \times 2^n \cdot n}$, and thus $\mathbf{L}^T \in \mathbb{R}^{2^n \cdot n \times 1}$, we find that $\mathbf{L}^T = \text{vec}(\mathbf{L})$. Substituting this back into the previous equation we achieve Equation (65).

E.2 Full Derivation of Equation (66).

Our goal is to transition from the equation,

$$[\mathbf{L} \text{vec}(\mathbf{P}_S^T \mathcal{X} \mathbf{P}_T)] = \mathbf{P}_S^T [\mathbf{L} \text{vec}(\mathcal{X})] \mathbf{P}_T \quad (64)$$

to the form,

$$\mathbf{P}_T \otimes \mathbf{P}_S \otimes \mathbf{P}_T \otimes \mathbf{P}_S \text{vec}(\mathbf{L}) = \text{vec}(\mathbf{L}). \quad (66)$$

Applying the property in Equation (74), after the reverse operation of the vectorization, namely,

$$[\text{vec}(\mathbf{ABC})] = [(\mathbf{C}^T \otimes \mathbf{A}) \text{vec}(\mathbf{B})] \quad (78)$$

on the right hand side of Equation (64), for

$$\mathbf{A} \triangleq \mathbf{P}_S^T; \quad (79)$$

$$\mathbf{B} \triangleq [\mathbf{L} \text{vec}(\mathcal{X})]; \quad (80)$$

$$\mathbf{C} \triangleq \mathbf{P}_T, \quad (81)$$

we obtain,

$$[\mathbf{L} \text{vec}(\mathbf{P}_S^T \mathcal{X} \mathbf{P}_T)] = [\mathbf{P}_T^T \otimes \mathbf{P}_S^T \mathbf{L} \text{vec}(\mathcal{X})]. \quad (82)$$

Thus, by omitting the reverse-vectorization operation,

$$\mathbf{L} \text{vec}(\mathbf{P}_S^T \mathcal{X} \mathbf{P}_T) = \mathbf{P}_T^T \otimes \mathbf{P}_S^T \mathbf{L} \text{vec}(\mathcal{X}). \quad (83)$$

Noting that $(\mathbf{P}_T^T \otimes \mathbf{P}_S^T)^{-1} = \mathbf{P}_T \otimes \mathbf{P}_S$, and multiplying by this inverse both sides (from the left), we obtain,

$$\mathbf{P}_T \otimes \mathbf{P}_S \mathbf{L} \text{vec}(\mathbf{P}_S^T \mathcal{X} \mathbf{P}_T) = \mathbf{L} \text{vec}(\mathcal{X}). \quad (84)$$

Applying, again, the property in Equation (74), we obtain,

$$\mathbf{P}_T \otimes \mathbf{P}_S \mathbf{L} \mathbf{P}_T^T \otimes \mathbf{P}_S^T \text{vec}(\mathcal{X}) = \mathbf{L} \text{vec}(\mathcal{X}). \quad (85)$$

Since this should be true for any $\mathcal{X} \in \mathbb{R}^{2^n \times n}$, we derive,

$$\mathbf{P}_T \otimes \mathbf{P}_S \mathbf{L} \mathbf{P}_T^T \otimes \mathbf{P}_S^T = \text{vec}(\mathbf{L}). \quad (86)$$

Again, applying Equation (74) on the left side, where,

$$\mathbf{A} \triangleq \mathbf{P}_T \otimes \mathbf{P}_S; \quad (87)$$

$$\mathbf{B} \triangleq \mathbf{L}; \quad (88)$$

$$\mathbf{C} \triangleq \mathbf{P}_T^T \otimes \mathbf{P}_S^T, \quad (89)$$

we get the following equality,

$$\mathbf{P}_T \otimes \mathbf{P}_S \mathbf{L} \mathbf{P}_T^T \otimes \mathbf{P}_S^T = \mathbf{P}_T \otimes \mathbf{P}_S \otimes \mathbf{P}_T \otimes \mathbf{P}_S \text{vec}(\mathbf{L}). \quad (90)$$

By substituting this to the left side of Equation (86) we obtain Equation (66).

E.3 Comparative Parameter Reduction in Linear Equivariant Layers

To demonstrate the effectiveness of our parameter-sharing scheme, which results from considering unordered tuples rather than ordered tuples, we present the following comparison. 3-IGNs [22] are structurally similar to our approach, with the main difference being that they consider indices as ordered tuples, while we consider them as sets. Both approaches use a total of six indices, as shown in the visualized block in Figure 3, making 3-IGNs a natural comparator. By leveraging our scheme, we reduce the number of parameters from 203 (the number of parameters in 3-IGNs) to just 35!

F Extended Experimental Section

F.1 Dataset Description

In this section we overview the eight different datasets considered; this is summarized in Table 5.

ZINC-12K and ZINC-FULL Datasets [32, 14, 10]. The ZINC-12K dataset includes 12,000 molecular graphs sourced from the ZINC database, a compilation of commercially available chemical compounds. These molecular graphs vary in size, ranging from 9 to 37 nodes, where each node represents a heavy atom, covering 28 different atom types. Edges represent chemical bonds and there are three types of bonds. The main goal when using this dataset is to perform regression analysis on the constrained solubility (logP) of the molecules. The dataset is divided into training, validation, and test sets with 10,000, 1,000, and 1,000 molecular graphs respectively. The full version, ZINC-FULL, comprises approximately 250,000 molecular graphs, ranging from 9 to 37 nodes and 16 to 84 edges per graph. These graphs also represent heavy atoms, with 28 distinct atom types, and the edges indicate bonds between these atoms, with four types of bonds present.

Table 5: Overview of the graph learning datasets.

Dataset	# Graphs	Avg. # nodes	Avg. # edges	Directed	Prediction task	Metric
ZINC-12K [32]	12,000	23.2	24.9	No	Regression	Mean Abs. Error
ZINC-FULL [32]	249,456	23.2	49.8	No	Regression	Mean Abs. Error
OGBG-MOLHIV [16]	41,127	25.5	27.5	No	Binary Classification	AUROC
OGBG-MOLBACE [16]	1513	34.1	36.9	No	Binary Classification	AUROC
OGBG-MOLESOL [16]	1,128	13.3	13.7	No	Regression	Root Mean Squ. Error
PEPTIDES-FUNC [9]	15,535	150.9	307.3	No	10-task Classification	Avg. Precision
PEPTIDES-STRUCT [9]	15,535	150.9	307.3	No	11-task Regression	Mean Abs. Error

OGBG-MOLHIV, OGBG-MOLBACE, OGBG-MOLESOL Datasets [16]. These datasets are used for molecular property prediction and have been adopted by the Open Graph Benchmark (OGB, MIT License) from MoleculeNet. They use a standardized featurization for nodes (atoms) and edges (bonds), capturing various chemophysical properties.

PEPTIDES-FUNC and PEPTIDES-STRUCT Datasets [9]. The PEPTIDES-FUNC and PEPTIDES-STRUCT datasets consist of atomic graphs representing peptides released with the Long Range Graph Benchmark (LRGB, MIT License). In PEPTIDES-FUNC, the task is to perform multi-label graph classification into ten non-exclusive peptide functional classes. Conversely, PEPTIDES-STRUCT is focused on graph regression to predict eleven three-dimensional structural properties of the peptides.

We note that for all datasets, we used the random splits provided by the public benchmarks.

F.2 Experimental Details

Implementation Details. Our implementation of Equation (2) is given by:

$$\mathcal{X}^{(l+1)} = \text{MLP} \left(\sum_{i=1}^3 \text{MPNN}^{(l+1,i)} (\mathcal{X}, \mathcal{A}_i) \right), \quad (91)$$

where $\mathcal{A}_1 = \mathcal{A}_G$, $\mathcal{A}_2 = \mathcal{A}_{\mathcal{T}(G)}$, and $\mathcal{A}_3 = \mathcal{A}_{\text{Equiv}}$.

For all considered datasets, namely, ZINC-12K, ZINC-FULL, OGBG-MOLHIV, OGBG-MOLBACE, and OGBG-MOLESOL, except for the PEPTIDES-FUNC and PEPTIDES-STRUCT datasets, we use a GINE [15] base encoder. Given an adjacency matrix \mathcal{A} , and defining $e_{(S',v'),(S,v)}$ to denote the edge features from node (S', v') to node (S, v) , it takes the following form:

$$\mathcal{X}(S, v) = \text{MLP} \left((1 + \epsilon) \cdot \mathcal{X}(S, v) + \sum_{(S',v') \sim_{\mathcal{A}} (S,v)} \text{ReLU}(\mathcal{X}(S', v') + e_{(S',v'),(S,v)}) \right). \quad (92)$$

We note that for the symmetry-based updates, we switch the ReLU to an MLP¹¹ to align with the theoretical analyses¹² (Appendix B), stating that we can implement the equivariant update developed in Section 4.2. A more thorough discussion regarding the implementation of the symmetry-based updates is given in Appendix F.4.

When experimenting with the PEPTIDES-FUNC and PEPTIDES-STRUCT datasets, we employ GAT [33] as our underlying MPNN to ensure a fair comparison with the random baseline—the random variant of Subgraphormer + PE [3]. To clarify, we consider the random variant of Subgraphormer + PE as a natural random baseline since it incorporates the information in the eigenvectors of the Laplacian (which we also do via the coarsening function). To maintain a fair comparison, we use a single vote for this random baseline, and maintained the same hyperparameters.

Our experiments were conducted using the PyTorch [29] and PyTorch Geometric [11] frameworks (resp. BSD and MIT Licenses), using a single NVIDIA L40 GPU, and for every considered experiment, we show the mean \pm std. of 3 runs with different random seeds. Hyperparameter tuning was performed utilizing the Weight and Biases framework [6] – see Appendix F.3. All our MLPs feature a single hidden layer equipped with a ReLU non-linearity function. For the encoding of atom numbers and bonds, we utilized learnable embeddings indexed by their respective numbers.

¹¹With the exception of the OGB datasets, to avoid overfitting.

¹²The theoretical analysis assumes the usage of an MLP for all three considered updates.

In the case of the OGBG-MOLHIV, OGBG-MOLESOL, OGBG-MOLBACE datasets, we follow Frasca et al. [12], therefore adding a residual connection between different layers. Additionally, for those datasets (except OGBG-MOLHIV), we used linear layers instead of MLPs inside the GIN layers. Moreover, for these four datasets, and for the PEPTIDES datasets, the following pooling mechanism was employed

$$\rho(\mathcal{X}) = \text{MLP} \left(\sum_S \left(\frac{1}{n} \sum_{v=1}^n \mathcal{X}(s, v) \right) \right). \quad (93)$$

For the PEPTIDES datasets, we also used a residual connection between layers.

F.3 HyperParameters

In this section, we detail the hyperparameter search conducted for our experiments. Besides standard hyperparameters such as learning rate and dropout, our specific hyperparameters are:

1. **Laplacian Dimension:** This refers to the number of columns used in the matrix U , where $L = U^T \lambda U$, for the spectral clustering in the coarsening function.
2. **SPD Dimension:** This represents the number of indices used in the node marking equation. To clarify, since $|S|$ might be large, we opt for using the first k indices that satisfy $i \in S$, sorted according to the SPD distance.

SPD Dimension. For the Laplacian dimension, we chose a fixed value of 10 for all bag sizes for both ZINC-12K and ZINC-FULL datasets. For OGBG-MOLHIV, we used a fixed value of 1, since the value 10 did not perform well. For the PEPTIDES datasets, we also used the value 1. For the OGBG-MOLESOL and OGBG-MOLBACE datasets, we searched over the two values $\{1, 2\}$.

Laplacian Dimension. For the Laplacian dimension, we searched over the values $\{1, 2\}$ for all datasets.

Standard Hyperparameters. For ZINC-12K, we used a weight decay of 0.0003 for all bag sizes, except for the full bag size, for which we used 0.0001.

All of the hyperparameter search configurations are presented in Table 6, and the selected hyperparameters are presented in Table 7.

Table 6: Hyperparameters search for CS-GNN.

Dataset	Bag size	Num. layers	Learning rate	Embedding size	Epochs	Batch size	Dropout	Laplacian dimension	SPD dimension
ZINC-12K	$T = 2$	6	0.0005	96	400	128	0	$\{1, 2\}$	10
ZINC-12K	$T \in \{3, 4, 5, 8, 18\}$	6	0.0007	96	400	128	0	$\{1, 2\}$	10
ZINC-12K	$T = \text{"full"}$	6	0.0007	96	500	128	0	$\{1, 2\}$	10
ZINC-FULL	$T = 4$	6	0.0007	96	400	128	0	$\{1, 2\}$	10
ZINC-FULL	$T = \text{"full"}$	6	$\{0.001, 0.0005\}$	96	500	128	0	$\{1, 2\}$	10
OGBG-MOLHIV	$T \in \{2, 5, \text{"full"}\}$	2	0.01	60	100	32	0.5	$\{1, 2\}$	1
OGBG-MOLESOL	$T \in \{2, 5, \text{"full"}\}$	3	0.001	60	100	32	0.3	$\{1, 2\}$	$\{1, 2\}$
OGBG-MOLBACE	$T \in \{2, 5, \text{"full"}\}$	$\{2, 3\}$	0.01	60	100	32	0.3	$\{1, 2\}$	$\{1, 2\}$
PEPTIDES-FUNC	$T = 30$	5	$\{0.01, 0.005\}$	96	200	128	0	$\{1, 2\}$	1
PEPTIDES-STRUC	$T = 30$	4	$\{0.01, 0.005\}$	96	200	128	0	$\{1, 2\}$	1

Optimizers and Schedulers. For the ZINC-12K and ZINC-FULL datasets, we employ the Adam optimizer paired with a ReduceLROnPlateau scheduler, factor set to 0.5, patience at 40¹³, and a minimum learning rate of 0. For the OGBG-MOLHIV dataset, we utilized the ASAM optimizer [21] without a scheduler. For both OGBG-MOLESOL and OGBG-MOLBACE, we employed a constant learning rate without any scheduler. Lastly, for the PEPTIDES-FUNC and PEPTIDES-STRUCT datasets, the AdamW optimizer was chosen in conjunction with a cosine annealing scheduler, incorporating 10 warmup epochs.

F.4 Implementation of Linear Equivariant and Invariant layers – Extended Section

In this section, in a more formal discussion, we specify how to integrate those invariant and equivariant layers to our proposed architecture. We start by drawing an analogy between parameter sharing in linear layers and the operation of an MPNN on a fully connected graph with edge features in the following lemma,

¹³For ZINC-12K, $T \in \{2, \text{"full"}\}$, we used a patience of 50.

Table 7: Chosen Hyperparameters for CS-GNN.

Dataset	Bag size	Num. layers	Learning rate	Embedding size	Epochs	Batch size	Dropout	Laplacian dimension	SPD dimension
ZINC-12K	$T = 2$	6	0.0005	96	400	128	0	1	10
ZINC-12K	$T = 3$	6	0.0007	96	400	128	0	2	10
ZINC-12K	$T = 4$	6	0.0007	96	400	128	0	1	10
ZINC-12K	$T = 5$	6	0.0007	96	400	128	0	1	10
ZINC-12K	$T = 8$	6	0.0007	96	400	128	0	1	10
ZINC-12K	$T = 18$	6	0.0007	96	400	128	0	1	10
ZINC-12K	$T = \text{"full"}$	6	0.0007	96	500	128	0	N/A	10
ZINC-FULL	$T = 4$	6	0.0007	96	400	128	0	1	10
ZINC-FULL	$T = \text{"full"}$	6	0.0005	96	500	128	0	N/A	N/A
OGBG-MOLHIV	$T = 2$	2	0.01	60	100	32	0.5	1	1
OGBG-MOLHIV	$T = 5$	2	0.01	60	100	32	0.5	1	1
OGBG-MOLHIV	$T = \text{"full"}$	2	0.01	60	100	32	0.5	N/A	N/A
OGBG-MOLESOL	$T = 2$	3	0.001	60	100	32	0.3	1	2
OGBG-MOLESOL	$T = 5$	3	0.001	60	100	32	0.3	1	2
OGBG-MOLESOL	$T = \text{"full"}$	3	0.001	60	100	32	0.3	N/A	N/A
OGBG-MOLBACE	$T = 2$	3	0.01	60	100	32	0.3	1	1
OGBG-MOLBACE	$T = 5$	3	0.01	60	100	32	0.3	1	2
OGBG-MOLBACE	$T = \text{"full"}$	3	0.01	60	100	32	0.3	N/A	N/A
PEPTIDES-FUNC	$T = 30$	5	0.005	96	200	128	0	1	1
PEPTIDES-STRUC	$T = 30$	4	0.01	96	200	128	0	1	1

Lemma F.1 (Parameter Sharing as MPNN). *Let $B_1, \dots, B_k : \mathbb{R}^{n \times n}$ be orthogonal matrices with entries restricted to 0 or 1, and let $W_1, \dots, W_k \in \mathbb{R}^{d \times d'}$ denote a sequence of weight matrices. Define $B_+ = \sum_{i=1}^k B_i$ and choose $z_1, \dots, z_k \in \mathbb{R}^{d^*}$ to be a set of unique vectors representing an encoding of the index set. The function, which represents an update via parameter sharing:*

$$f(X) = \sum_{i=1}^k B_i X W_i, \quad (94)$$

can be implemented by a stack of MPNN layers of the following form [13],

$$m_u^l = \sum_{v \in N_{B_+}(u)} M^l(X_v^l, e_{u,v}), \quad (95)$$

$$X_u^{l+1} = U^l(X_v^l, m_v^l), \quad (96)$$

where U^l, M^l are multilayer perceptrons (MLPs). The inputs to this MPNN are the adjacency matrix B_+ , node feature vector X , and edge features – the feature of edge (u, v) is given by:

$$e_{u,v} = \sum_{i=1}^k z_i \cdot B_i(u, v). \quad (97)$$

Here, $B_i(u, v)$ denotes the (u, v) entry to matrix B_i .

The proof is given in Appendix G.

Thus, our implementation for the global update is as follows,

$$\mathcal{X}(S, i) = \text{MLP} \left((1 + \epsilon) \cdot \mathcal{X}(S, i) + \sum_{(S', i') \sim \mathcal{A}_{\text{Equiv}}(S, i)} \text{MLP} \left(\mathcal{X}(S', i') + e_{(S', i'), (S, i)} \right) \right), \quad (98)$$

where $e_{(S', i'), (S, i)} = \sum_{\Gamma} z_{\Gamma} \cdot \mathbf{B}_{S, i; S', i'}^{\Gamma}$ and z_{Γ} are orthogonal 1-hot vectors for different Γ 's. The connectivity $\mathcal{A}_{\text{Equiv}}$ is such that $\mathcal{A}_{\text{Equiv}}(S, v, S', v')$ contains the value one iff $v \in S, v = v'$. This corresponds to choosing only several Γ 's in the partition, and since each Γ is invariant to the permutation, this choice still maintains equivariance.

F.5 Additional Results

ZINC-FULL. Below, we present our results on the ZINC-FULL dataset for a bag size of $T = 4$ and the full-bag. For the bag size $T = 4$, we benchmark against MAG-GNN [20], which in their experiments used the best out of the bag sizes $T \in \{2, 3, 4\}$; however, they did not specify which one performed the best. The results are summarized in Table 8.

Table 8: Comparison over the ZINC-FULL molecular dataset under 500k parameter budget. The best performing method is highlighted in **blue**, while the second best is highlighted in **red**.

Model ↓ / Dataset →	ZINC-FULL (MAE ↓)
MAG-GNN [20] ($T = 4$)	0.030 ±0.002
Ours ($T = 4$)	0.027 ±0.002
GNN-SSWL [39] ($T = \text{"full"}$)	0.026±0.001
GNN-SSWL+ [39] ($T = \text{"full"}$)	0.022±0.001
Subgraphormer [3] ($T = \text{"full"}$)	0.020 ±0.002
Subgraphormer + PE [3] ($T = \text{"full"}$)	0.023±0.001
Ours ($T = \text{"full"}$)	0.021 ±0.001

Table 9: Test results on the ZINC-12K molecular dataset under 500k parameter budget. The top two results are reported as **First** and **Second**.

Method	Bag size	ZINC (MAE ↓)
GCN [19]	$T = 1$	0.321 ± 0.009
GIN [36]	$T = 1$	0.163 ± 0.004
OSAN [30]	$T = 2$	0.177 ± 0.016
Random [20]	$T = 2$	0.131 ± 0.005
PL [5]	$T = 2$	0.120 ± 0.003
Mag-GNN [20]	$T = 2$	0.106 ± 0.014
Ours	$T = 2$	0.109 ± 0.005
Random [20]	$T = 3$	0.124 ± N/A
Mag-GNN [20]	$T = 3$	0.104 ± N/A
Ours	$T = 3$	0.096 ± 0.005
Random [20]	$T = 4$	0.125 ± N/A
Mag-GNN [20]	$T = 4$	0.101 ± N/A
Ours	$T = 4$	0.090 ± 0.003
Random [5]	$T = 5$	0.113 ± 0.006
PL [5]	$T = 5$	0.109 ± 0.005
Ours	$T = 5$	0.095 ± 0.003
Random [5]	$T = 8$	0.102 ± 0.003
PL [5]	$T = 8$	0.097 ± 0.005
Ours	$T = 8$	0.094 ± 0.006
Ours	$T = 18$	0.082 ± 0.003
NGNN [40]	Full	0.111±0.003
DS-GNN [4]	Full	0.116±0.009
DSS-GNN [4]	Full	0.102±0.003
GNN-AK [41]	Full	0.105±0.010
GNN-AK+ [41]	Full	0.091±0.002
SUN [12]	Full	0.083±0.003
OSAN [30]	Full	0.154±0.008
GNN-SSWL+ [39]	Full	0.070 ± 0.005
Subgraphormer [3]	Full	0.067 ± 0.007
Subgraphormer+PE [3]	Full	0.063 ± 0.001
Ours	Full	0.062 ± 0.0007

ZINC-12K – additional results. We present all the results from Figure 2, along with some additional ones, in Table 9.

Runtime comparison. We compare the training time and prediction performance on the ZINC-12K dataset. For all methods, we report the training and inference times on the entire training and test sets, respectively, using a batch size of 128. Our experiments were conducted using an NVIDIA L40 GPU, while for the baselines, we used the timing reported in [5], which utilized an RTX A6000 GPU. The runtime comparison is presented in Table 10.

Table 10: Run time comparison over the ZINC-12K dataset. Time taken at train for one epoch and at inference on the test set. All values are in milliseconds.

Method	Train time (for a single epoch; ms)	Test time (ms)	MAE ↓
GIN [36]	1370.10 ± 10.97	84.81 ± 0.26	0.163 ± 0.004
OSAN [30] ($T = 2$)	2964.46 ± 30.36	227.93 ± 0.21	0.177 ± 0.016
PL [5] ($T = 2$)	2489.25 ± 9.42	150.38 ± 0.33	0.120 ± 0.003
Ours ($T = 2$)	2764.60 ± 234	383.14 ± 15.74	0.109 ± 0.005

G Proofs

G.1 Proofs of Appendix B

We first state the memorization theorem, proven in [37], which will be heavily used in a lot of the proofs in this section.

Theorem G.1 (Memorization Theorem). *Consider a dataset $\{x_j, y_j\}_{j=1}^N \in \mathbb{R}^d \times \mathbb{R}^{d_y}$, with each x_j being distinct and every $y_j \in \{0, 1\}^{d_y}$. There exists a 4-layer fully connected ReLU neural network $f_\theta : \mathbb{R}^d \rightarrow \mathbb{R}^{d_y}$ that perfectly maps each x_j to its corresponding y_j , i.e., $f_\theta(x_j) = y_j$ for all j .*

We now restate and prove the propositions and Lemmas of Appendix B.

Lemma B.1 (Parameter Sharing as MPNN). *Let $B_1, \dots, B_k : \mathbb{R}^{n \times n}$ be orthogonal matrices with entries restricted to 0 or 1, and let $W_1, \dots, W_k \in \mathbb{R}^{d \times d'}$ denote a sequence of weight matrices. Define $B_+ = \sum_{i=1}^k B_i$ and choose $z_1, \dots, z_k \in \mathbb{R}^{d^*}$ to be a set of unique vectors representing an encoding of the index set. The function that represents an update via parameter sharing:*

$$f(X) = \sum_{i=1}^k B_i X W_i, \quad (18)$$

can be implemented on any finite family of graphs \mathcal{G} , by a stack of MPNN layers of the following form [13],

$$m_v^l = \sum_{u \in N_{B_+}(v)} M^l(X_u^l, e_{u,v}), \quad (19)$$

$$X_v^{l+1} = U^l(X_v^l, m_v^l), \quad (20)$$

where U^l, M^l are multilayer perceptrons (MLPs). The inputs to this MPNN are the adjacency matrix B_+ , node feature vector X , and edge features – the feature of edge (u, v) is given by:

$$e_{u,v} = \sum_{i=1}^k z_i \cdot B_i(u, v). \quad (21)$$

Here, $B_i(u, v)$ denotes the (u, v) entry to matrix B_i .

Proof. Since we are concerned only with input graphs G from a finite family of graphs (where "finite" means that the maximal graph size is bounded and all possible node and edge feature values come from a finite set), we assume that for any $v \in [n]$, $i \in [k]$, both the input feature vectors $X_v \in \mathbb{R}^d$ and the encoding vectors $z_i \in \mathbb{R}^{d^*}$ are one-hot encoded. We aim to show that under these assumptions, any function $f(\cdot)$ of the form 94 can be realized through a single-layer update detailed in Equations 96, 95, where M is a 4 layer MLP, and U is a single linear layer. The proof involves the following steps:

1. Compute $[B_1 X, \dots, B_k X]$ using the message function M .
2. Compute $f(X)$ using the update function U .

Step 1: We notice that for every $i \in [k]$, $v \in [n]$ we have:

$$(B_i X)_v = \sum_{B_i(v,u)=1} X_u = \sum_{u \in N_{B_+}(v)} X_u \cdot \mathbf{1}_{z_i}(e_{u,v}). \quad (99)$$

Here $\mathbf{1}_{z_i}$ is the indicator function of the set $\{z_i\}$. We notice that since X_u and z_i are one-hot encoded, there is a finite set of possible values for the pair $(X_u, e_{u,v})$. In addition, the function:

$$\text{enc}(X_u, e_{u,v}) = [X_u \cdot \mathbf{1}_{z_1}(e_{u,v}), \dots, X_u \cdot \mathbf{1}_{z_k}(e_{u,v})] \quad (100)$$

outputs vectors in the set $\{0, 1\}^{d \times k}$. Thus, employing the memorization theorem G.1, we define a dataset $\{x_j, y_j\}_{j=1}^N$ by taking the x_j s to be all possible (distinct) values of $(X_u, e_{u,v})$ with each

corresponding y_i being the output $\text{enc}(x_i)$. We note that there are finitely many such values as both X_u and $e_{u,v}$ are one-hot encoded. The theorem now tells us that there exists a 4-layer fully connected ReLU neural network M such that:

$$M(X_u, e_{u,v}) = \text{enc}(X_u, e_{u,v}). \quad (101)$$

and so, equation 99 implies:

$$m_v = \sum_{u \in N_{B+}(v)} M(X_u, e_{u,v}) = [(B_1 X)_v, \dots, (B_k X)_v]. \quad (102)$$

Step 2: Define $P_i : \mathbb{R}^{k \times d} \rightarrow \mathbb{R}^d$ as the projection operator, extracting coordinates $d \cdot i + 1$ through $d \cdot (i + 1)$ from its input vector:

$$P_i(V) = V|_{d \cdot i + 1 : d \cdot (i + 1)}. \quad (103)$$

We define the update function to be the following linear map:

$$U(X_v, m_v) = \sum_{i=1}^k P_i(m_v) W_i. \quad (104)$$

Combining equations 102 and 104 we get:

$$\tilde{X}_v = U(X_v, m_v) = \sum_{i=1}^k (B_i X)_v \cdot W_i = f(X)_v. \quad (105)$$

□

Proposition B.1 (Equivalence of General Layer and Implemented Layer). *Let $\mathcal{T}(\cdot)$ be a coarsening function, π be a generalized node marking policy, and \mathcal{G} be a finite family of graphs. Applying a stack of t general layer updates as defined in Equation 15 to the node feature map $\mathcal{X}(S, v)$ induced by $\pi(G, \mathcal{T})$, can be effectively implemented by applying a stack of t layer updates specified in Equations 29 and 30 to $\mathcal{X}(S, v)$. Additionally, the depths of all MLPs that appear in 29 and 30 can be bounded by 4.*

Proof. For convenience, let us first restate the general layer update:

$$\begin{aligned} \mathcal{X}^{t+1}(S, v) = f^t \Big(& \mathcal{X}^t(S, v), \\ & \text{agg}_1^t \{ \{ \mathcal{X}^t(S, v'), e_{v, v'} \} \mid v' \sim_G v \}, \\ & \text{agg}_2^t \{ \{ \mathcal{X}^t(S', v), \tilde{e}_{S, S'} \} \mid S' \sim_{G^T} S \}, \\ & \text{agg}_3^t \{ \{ \mathcal{X}^t(S', v), z(S, v, S', v) \} \mid S' \in V^T \text{ s.t. } v \in S' \}, \\ & \text{agg}_4^t \{ \{ \mathcal{X}^t(S, v'), z(S, v, S, v') \} \mid v' \in V \text{ s.t. } v' \in S \} \Big), \end{aligned} \quad (15)$$

as well as the two step implemented layer update:

$$\mathcal{X}_i^t(S, v) = U_i^t \left((1 + \epsilon_i^t) \cdot \mathcal{X}^t(S, v) + \sum_{(S', v') \sim_{A_i}(S, v)} M^t(\mathcal{X}^t(S', v') + e_i(S, v, S', v')) \right). \quad (29)$$

$$\mathcal{X}^{t+1}(S, v) = U_{\text{fin}}^t \left(\sum_{i=1}^4 \mathcal{X}_i^t(S, v) \right). \quad (30)$$

We aim to demonstrate that any general layer, which updates the node feature map $\mathcal{X}^t(S, v)$ at layer t to node feature map $\mathcal{X}^{t+1}(S, v)$ at layer $t + 1$ as described in equation 15, can be effectively implemented using the layer update processes outlined in equations 29 and 30.

As we are concerned only with input graphs belonging to the finite graph family \mathcal{G} (where "finite" indicates that the maximal graph size is bounded and all node and edge features have a finite set of possible values), we assume that the values of the node feature map $\mathcal{X}^t(S, v)$ and the edge feature vectors $e_i(S, v, S', v')$ are represented as one-hot vectors in \mathbb{R}^k . We also assume that the parameterized functions f^t and $\text{agg}_1^t, \dots, \text{agg}_4^t$, which are applied in Equation 15 outputs one-hot vectors. Finally, we assume that there exists integers d, d^* , such that the node feature map values are supported on coordinates $1, \dots, d$, the edge feature vectors are supported on coordinates $d+1, \dots, d+d^*$, and coordinates $d+d^*+1, \dots, k$ are used as extra memory space, with:

$$k > d \times d^* + d + d^*. \quad (106)$$

We note that the last assumption can be easily achieved using padding. The proof involves the following steps:

1. For $i = 1, \dots, 4$, Use the term:

$$m_i^t = \sum_{(S', v') \sim_{A_i}(S, v)} M^t(\mathcal{X}^t(S', v') + e_i(S, v, S', v')) \quad (107)$$

to uniquely encode:

$$\{(\mathcal{X}^t(S', v'), e_i(S, v, S', v')) \mid (S', v') \sim_{A_i}(S, v)\}. \quad (108)$$

2. Use the term:

$$\mathcal{X}_*^t = \sum_{i=1}^4 \mathcal{X}_i^t(S, v) \quad (109)$$

to uniquely encode the input of f^t as a whole.

3. Implement the parameterized function f^t .

Step 1: Since we assume that node feature map values and edge feature vectors are supported on orthogonal sub-spaces of \mathbb{R}^k , the term:

$$\mathcal{X}^t(S, v) + e_i(S, v, S', v') \quad (110)$$

uniquely encodes the value of the tuple:

$$(\mathcal{X}^t(S, v), e_i(S, v, S', v')). \quad (111)$$

Since $\mathcal{X}^t(S, v)$ is a one-hot encoded vector with d possible values, while $e_i(S, v, S', v')$ is a one-hot encoded vector with d^* possible values, their sum has $d \cdot d^*$ possible values. Thus there exists a function:

$$\text{enc} : \mathbb{R}^k \rightarrow \mathbb{R}^k$$

which encodes each such possible value as a one-hot vector in \mathbb{R}^k supported on the last $k - d - d^*$ coordinates (this is possible because of equation 106). Now, employing theorem G.1, we define the x_j s as all possible (distinct) values of 110, with each corresponding y_j being the output $\text{enc}(x_j)$. The theorem now tells us that there exists a 4-layer fully connected ReLU neural network capable of implementing the function $\text{enc}(\cdot)$. We choose M^t to be this network. Now since m_i^t , defined in equation 107 is a sum of one-hot encoded vectors, it effectively counts the number of each possible value in the set 108. This proves step 1.

Step 2: First, we note that:

$$\begin{aligned} & \{(\mathcal{X}^t(S, v'), e_{v, v'}) \mid v' \sim_G v\} \\ &= \{(\mathcal{X}^t(S', v'), e_G(S, v, S', v')) \mid (S, v) \sim_{A_G}(S', v')\} \end{aligned} \quad (112)$$

$$\begin{aligned} & \{(\mathcal{X}^t(S', v), e_{s', s}) \mid S' \sim_{\mathcal{T}(G)} S\} \\ &= \{(\mathcal{X}^t(S', v'), e_{\mathcal{T}(G)}(S, v, S', v')) \mid (S, v) \sim_{A_{\mathcal{T}(G)}}(S', v')\} \end{aligned} \quad (113)$$

$$\begin{aligned} & \{(\mathcal{X}^t(S', v), z(S, v, S', v')) \mid v \in S'\} \\ &= \{(\mathcal{X}^t(S', v'), e_{P_1}(S, v, S', v')) \mid (S, v) \sim_{A_{P_1}}(S', v')\} \end{aligned} \quad (114)$$

$$\begin{aligned} & \{ \{ \mathcal{X}^t(S, v'), z(S, v, S', v') \} \mid v' \in S \} \\ &= \{ \{ \mathcal{X}^t(S', v'), e_{P_2}(S, v, S', v') \} \mid (S, v) \sim_{A_{P_2}} (S', v') \} \end{aligned} \quad (115)$$

Now, since m_i^t and $\mathcal{X}^t(S, v)$ are supported on orthogonal sub-spaces of \mathbb{R}^k , the sum $\mathcal{X}^t(S, v) + m_i^t$ uniquely encodes the value of:

$$(\mathcal{X}^t(S, v), \{ \{ \mathcal{X}^t(s, v), e_i(S, v, S', v') \} \mid (S, v) \sim_{A_i} (S', v') \}). \quad (116)$$

Thus, we choose $\epsilon_1^t, \dots, \epsilon_4^t$ to be all zeroes. To compute the aggregation functions $\text{agg}_1^t, \dots, \text{agg}_4^t$ using these unique encodings, and to avoid repetition of the value $\mathcal{X}^t(S, v)$, we define auxiliary functions $\text{agg}_i^t : \mathbb{R}^k \rightarrow \mathbb{R}^{k_i}$ for $i = 1, \dots, 4$ as follows:

$$\text{agg}_1^t(\mathcal{X}^t(S, v) + m_1^t) = (\mathcal{X}^t(S, v), \text{agg}_1^t(\{ \{ \mathcal{X}^t(S, v'), e_1(S, v, S', v') \} \mid (S, v) \sim_{A_1} (S', v') \})) \quad (117)$$

and for $i > 1$:

$$\text{agg}_i^t(\mathcal{X}^t(S, v) + m_i^t) = \text{agg}_i^t(\{ \{ \mathcal{X}^t(s, v), e_i(S, v, S', v') \} \mid (S, v) \sim_{A_i} (S', v') \}). \quad (118)$$

Here, since we avoided repeating the value of $\mathcal{X}^t(S, v)$ by only adding it to the output of $\text{agg}_1^t(\cdot)$, the expression:

$$(\text{agg}_1^t(\mathcal{X}^t(S, v) + m_1^t), \dots, \text{agg}_4^t(\mathcal{X}^t(S, v) + m_4^t)) \quad (119)$$

is exactly equal to the input of f^t . In addition, since the function agg_i^t outputs one-hot encoded vectors, and the vector $\mathcal{X}^t(S, v)$ is one-hot encoded, the output of agg_i^t is always within the set $\{0, 1\}^{k_i}$. Now for any input vector $X \in \mathbb{R}^k$ define:

$$V_1^t(X) = (\text{agg}_1^t(X), 0_{k_2}, 0_{k_3}, 0_{k_4}). \quad (120)$$

$$V_2^t(X) = (0_{k_1}, \text{agg}_2^t(X), 0_{k_3}, 0_{k_4}). \quad (121)$$

$$V_3^t(X) = (0_{k_1}, 0_{k_2}, \text{agg}_3^t(X), 0_{k_4}). \quad (122)$$

$$V_4^t(X) = (0_{k_1}, 0_{k_2}, 0_{k_3}, \text{agg}_4^t(X)). \quad (123)$$

We note that since the output of agg_i^t is always within the set $\{0, 1\}^{k_i}$, the outputs of V_i^t is always within $\{0, 1\}^{k_1 + \dots + k_4}$. Now for $i = 1, \dots, 4$, employing theorem G.1 we define a dataset $\{x_j, y_j\}_{j=1}^N$ by taking the x_j s as all possible (distinct) values of $\mathcal{X}^t(S, v) + m_i^t$, with each corresponding y_j being the output $V_i^t(x_j)$. We note that there are finitely many such values as both $\mathcal{X}^t(S, v)$ and m_i^t are one-hot encoded vectors. The theorem now tells us that there exists a 4-layer fully connected ReLU neural network capable of implementing the function $V_i^t(\cdot)$. We choose U_i^t to be this network. Equations 120 - 123 now give us:

$$\sum_{i=1}^4 \mathcal{X}_i^t(S, v) = (\text{agg}_1^t(\mathcal{X}^t(S, v) + m_1^t), \dots, \text{agg}_4^t(\mathcal{X}^t(S, v) + m_4^t)). \quad (124)$$

which as stated before, is exactly the input to f^t . This proves step 2.

Step 3: We employ theorem G.1 for one final time, defining a dataset $\{x_j, y_j\}_{j=1}^N$ by taking the x_j s as all possible (distinct) values of:

$$\sum_{i=1}^4 \mathcal{X}_i^t(S, v)$$

(which we showed is a unique encoding to the input of $f^t(\cdot)$), with each corresponding y_j being the output $f^t(x_j)$. We note that Given the finite nature of our graph set, there are finitely many such values. Recalling that $f^t(\cdot)$ outputs one-hot encoded vectors, The theorem now tells us that there exists a 4-layer fully connected ReLU neural network capable of implementing the function $f^t(\cdot)$. We choose U_{fin}^t to be this network. This completes the proof. \square

G.2 Proofs of Appendix C

Proposition C.1 (Equal Expressivity of Node Marking Policies). *For any coarsening function $\mathcal{T}(\cdot)$ the following holds:*

$$\text{CS-GNN}(\mathcal{T}, \pi_S) = \text{CS-GNN}(\mathcal{T}, \pi_{SS}) = \text{CS-GNN}(\mathcal{T}, \pi_{MD}). \quad (36)$$

Proof. Let $\Pi = \{\pi_S, \pi_{SS}, \pi_{MD}\}$ be the set of all relevant node initialization policies, and assume for simplicity that our input graphs have no node features (the proof can be easily adjusted to account for the general case). For each $\pi \in \Pi$, let $\mathcal{X}^\pi(S, v)$ denote the node feature map induced by general node marking policy π , as per Definition C.1. We notice it is enough to prove for each $\pi_1, \pi_2 \in \Pi$ that $\mathcal{X}^{\pi_1}(S, v)$ can be implemented by updating $\mathcal{X}^{\pi_2}(S, v)$ using a stack of T layers of type 54. Thus, we prove the following four cases:

- Node + Size Marking \Rightarrow Simple Node Marking.
- Minimum Distance \Rightarrow Simple Node Marking.
- Simple Node Marking \Rightarrow Node + Size Marking.
- Simple Node Marking \Rightarrow Minimum Distance.

Node + Size Marking \Rightarrow Simple Node Marking:

In this case, we aim to update the node feature map:

$$\mathcal{X}^0(S, v) = \mathcal{X}^{\pi_{SS}}(S, v) = \begin{cases} (1, |S|) & v \in S \\ (0, |S|) & v \notin S. \end{cases} \quad (125)$$

We notice that:

$$\mathcal{X}^0(S, v) = \langle (1, 0), \mathcal{X}^{\pi_S}(S, v) \rangle, \quad (126)$$

where $\langle \cdot, \cdot \rangle$ denotes the standard inner product in \mathbb{R}^2 . Using a CS-GNN update as per equation 15, with the update function:

$$f^1(\mathcal{X}^0(S, v), \cdot, \cdot, \cdot, \cdot) = \langle (1, 0), \mathcal{X}^0(S, v) \rangle, \quad (127)$$

where $f(a, \cdot, \cdot, \cdot, \cdot)$ indicates that the function f depends solely on the parameter a , we obtain:

$$\mathcal{X}^1(S, v) = f^1(\mathcal{X}^0(S, v), \cdot, \cdot, \cdot, \cdot) = \mathcal{X}^{\pi_S}(S, v). \quad (128)$$

This implies that for any coarsening function $\mathcal{T}(\cdot)$, the following holds:

$$\text{CS-GNN}(\mathcal{T}, \pi_S) \subseteq \text{CS-GNN}(\mathcal{T}, \pi_{SS}). \quad (129)$$

Minimum Distance \Rightarrow Simple Node Marking:

In this case, we aim to update the node feature map:

$$\mathcal{X}^0(S, v) = \mathcal{X}^{\pi_{MD}}(S, v) = \min_{u \in S} d_G(u, v) \quad (130)$$

We notice that:

$$\mathcal{X}^S(S, v) = g(\mathcal{X}^0(S, v)) \quad (131)$$

where $g : \mathbb{R} \rightarrow \mathbb{R}$ is any continuous function such that:

1. $g(x) = 1 \ \forall x > \frac{1}{2}$,
2. $g(x) = 0 \ \forall x < \frac{1}{4}$.

Using a CS-GNN update as per equation 15, with the update function:

$$f^1(\mathcal{X}^0(S, v), \cdot, \cdot, \cdot, \cdot) = g(\mathcal{X}^0(S, v)), \quad (132)$$

we obtain:

$$\mathcal{X}^1(S, v) = f^1(\mathcal{X}^0(S, v), \cdot, \cdot, \cdot, \cdot) = \mathcal{X}^{\pi_S}(S, v). \quad (133)$$

This implies that for any coarsening function $\mathcal{T}(\cdot)$ the following holds:

$$\text{CS-GNN}(\mathcal{T}, \pi_S) \subseteq \text{CS-GNN}(\mathcal{T}, \pi_{\text{MD}}). \quad (134)$$

Simple Node Marking \Rightarrow Node + Size Marking: In this case, we aim to update the node feature map:

$$\mathcal{X}^0(S, v) = \mathcal{X}^{\pi_S}(S, v) = \begin{cases} 1 & v \in S \\ 0 & v \notin S. \end{cases} \quad (135)$$

We notice that:

$$\sum_{v' \in S} \mathcal{X}^0(S, v') = |S|. \quad (136)$$

Using a CS-GNN update as per Equation (15), with aggregation function:

$$\text{agg}_4^l \{ \{ (\mathcal{X}^0(S, v'), z(S, v, S, v')) \mid v' \in S \} \} = \sum_{v' \in S} \mathcal{X}^0(S, v'), \quad (137)$$

and update function:

$$f^1 \left(\mathcal{X}^0(S, v), \cdot, \cdot, \cdot, \sum_{v' \in S} \mathcal{X}^0(S, v') \right) = \left(\mathcal{X}^0(S, v), \sum_{v' \in S} \mathcal{X}^0(S, v') \right), \quad (138)$$

we obtain:

$$\mathcal{X}^1(S, v) = f^1 \left(\mathcal{X}^0(S, v), \cdot, \cdot, \cdot, \sum_{v' \in S} \mathcal{X}^0(S, v') \right) = \mathcal{X}^{\pi_{SS}}(S, v). \quad (139)$$

This implies that for any coarsening function $\mathcal{T}(\cdot)$ the following holds:

$$\text{CS-GNN}(\mathcal{T}, \pi_{SS}) \subseteq \text{CS-GNN}(\mathcal{T}, \pi_S). \quad (140)$$

Simple Node Marking \Rightarrow Minimum Distance:

In this case, we aim to update the node feature map:

$$\mathcal{X}^0(S, v) = \mathcal{X}^{\pi_S}(S, v) = \begin{cases} 1 & v \in S \\ 0 & v \notin S. \end{cases} \quad (141)$$

We shall prove that $\mathcal{X}^{\pi_{\text{MD}}}$ can be expressed by updating $\mathcal{X}^0(S, v)$ with a stack of CS-GNN layers. We do this by inductively showing that this procedure can express the following auxiliary node feature maps:

$$\mathcal{X}_*^t(S, v) = \begin{cases} \min_{v' \in S} d_G(v, v') + 1 & \min_{v' \in S} d_G(v, v') \leq t \\ 0 & \text{otherwise.} \end{cases} \quad (142)$$

We notice first that:

$$\mathcal{X}^0(S, v) = \mathcal{X}_*^0(S, v). \quad (143)$$

Now for the induction step, assume that there exists a stack of t CS-GNN layers such that:

$$\mathcal{X}^t(S, v) = \mathcal{X}_*^t(S, v). \quad (144)$$

We observe that equation:

$$\min_{v' \in S} d_G(v, v') = t + 1 \quad (145)$$

holds if and only if the following two conditions are met:

$$\min_{v' \in S} d_G(v, v') > t \quad (146)$$

$$\exists u \in N_G(v) \text{ s.t. } \min_{u' \in S} d_G(u, u') = t. \quad (147)$$

Equations 142 imply:

$$\min_{v' \in S} d_G(v, v') > t \Leftrightarrow \mathcal{X}^t(S, v) = 0. \quad (148)$$

In addition, since the node feature map $\mathcal{X}^t = \mathcal{X}_*^t$ is bounded by $t + 1$, Equation (142) implies:

$$\exists u \in N_G(v) \text{ s.t. } \min_{u' \in S} d_G(u, u') = t \Leftrightarrow \max\{\mathcal{X}^t(s, u) \mid v \sim_G u\} = t + 1. \quad (149)$$

Now, let $g_t : \mathbb{R}^2 \rightarrow \mathbb{R}$ be any continuous function such that for every pair of natural numbers $a, b \in \mathbb{N}$:

1. $g_t(a, b) = t + 2$ if $a = 0, b = t + 1$,
2. $g_t(a, b) = a$ otherwise.

Equations 145 - 149 imply:

$$\mathcal{X}_*^{t+1}(S, v) = g_t(\mathcal{X}^t(S, v), \max\{\mathcal{X}^t(s, u) \mid v \sim_G u\}). \quad (150)$$

Using a CS-GNN update as per Equation (15), with aggregation function:

$$\text{agg}_1^t(\{\mathcal{X}^t(S, v'), e_{v, v'} \mid v' \sim_G v\}) = \max_{v' \sim_G v} \mathcal{X}^t(S, v'). \quad (151)$$

and update function:

$$f^t(\mathcal{X}^t(S, v), \max_{v' \sim_G v} \mathcal{X}^t(S, v'), \cdot, \cdot, \cdot) = g_t(\mathcal{X}^t(S, v), \max_{v' \sim_G v} \mathcal{X}^t(S, v')) \quad (152)$$

we obtain:

$$\mathcal{X}^{t+1}(S, v) = f^t(\mathcal{X}^t(S, v), \max_{v' \sim_G v} \mathcal{X}^t(S, v'), \cdot, \cdot, \cdot) = \mathcal{X}_*^{t+1}(S, v). \quad (153)$$

This completes the induction step. Now, let \mathcal{G} be a finite family of graphs, whose maximal vertex size is n . We notice that:

$$\mathcal{X}^{\pi_{\text{MD}}}(S, v) = \mathcal{X}_*^n(S, v) - 1, \quad (154)$$

Which implies that there exists a stack of n CS-GNN layers such that:

$$\mathcal{X}^0(S, v) = \mathcal{X}^{\pi_{\text{S}}}(S, v) \quad \text{and} \quad \mathcal{X}^n(S, v) = \mathcal{X}^{\pi_{\text{MD}}}(S, v). \quad (155)$$

This implies:

$$\text{CS-GNN}(\mathcal{T}, \pi_{\text{MD}}) \subseteq \text{CS-GNN}(\mathcal{T}, \pi_{\text{S}}). \quad (156)$$

This concludes the proof. \square

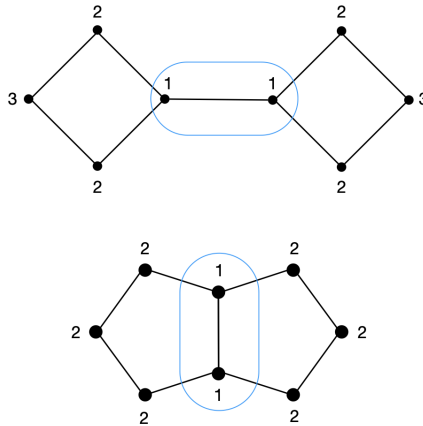


Figure 5: Graphs G and H defined in the proof of Proposition C.2. In each graph, the circle marks the single super-node induced by \mathcal{T} , while the number next to each node u is the maximal SPD between u and the nodes that compose the super-node.

Proposition C.2 (Expressivity of Learned Distance Policy). *For any coarsening function $\mathcal{T}(\cdot)$ the following holds:*

$$\text{CS-GNN}(\mathcal{T}, \pi_S) \subseteq \text{CS-GNN}(\mathcal{T}, \pi_{LD}). \quad (37)$$

In addition, for some choices of $\mathcal{T}(\cdot)$ the containment is strict.

Proof. First, since we are concerned with input graphs belonging to a finite graph family \mathcal{G} , the learned function $\phi(\cdot)$ implemented by an MLP can express any continuous function on \mathcal{G} . This follows from Theorem G.1 (see the proof of Proposition B.1 for details). By choosing $\phi = \min(\cdot)$ in equation 35, it is clear that for any coarsening function $\mathcal{T}(\cdot)$ we have:

$$\text{CS-GNN}(\mathcal{T}, \pi_S) = \text{CS-GNN}(\mathcal{T}, \pi_{MD}) \subseteq \text{CS-GNN}(\mathcal{T}, \pi_{LD}). \quad (157)$$

We now construct a coarsening function $\mathcal{T}(\cdot)$ along with two graphs, G and H , and demonstrate that there exists a function in $\text{CS-GNN}(\mathcal{T}, \pi_{LD})$ that can separate G and H . However, every function in $\text{CS-GNN}(\mathcal{T}, \pi_S)$ cannot separate the two.

For an input graph $G = (V, E)$ define:

$$\mathcal{T}(G) = \{\{u \in V \mid \deg_G(u) = 3\}\}. \quad (158)$$

i.e., $\mathcal{T}(\cdot)$ returns a single super-node composed of all nodes with degree 3. Now, define $G = (V_G, E_G)$ as the graph obtained by connecting two cycles of size four by adding an edge between a single node from each cycle. Additionally, define $H = (V_H, E_H)$ as the graph formed by joining two cycles of size five along one of their edges. See Figure 5 for an illustration of the two graphs. By choosing $\phi = \max(\cdot)$ in equation 35 a quick calculation shows that:

$$\sum_{S \in V_{\mathcal{T}(G)}} \sum_{v \in V_G} \mathcal{X}^{\pi_{LD}}(S, v) = 16, \quad (159)$$

while:

$$\sum_{S \in V_{\mathcal{T}(H)}} \sum_{v \in V_H} \mathcal{X}^{\pi_{LD}}(S, v) = 14. \quad (160)$$

Refer to Figure 5 for more details. Observe that:

$$f(G) = \sum_{s \in V_{\mathcal{T}(H)}} \sum_{u \in V_H} \mathcal{X}^{\pi_{LD}}(S, v) \in \text{CS-GNN}(\mathcal{T}, \pi_{LD}) \quad (161)$$

Thus it is enough to show that:

$$f(G) = f(H), \quad \forall f \in \text{CS-GNN}(\mathcal{T}, \pi_S). \quad (162)$$

To achieve this, we use the layer update as per Definition B.2, which was demonstrated in Proposition B.1 to be equivalent to the general equivariant message passing update in Definition A.5. First, we observe that the graphs G and H are WL-indistinguishable. We then observe that since $|V^{\mathcal{T}}| = 1$, the graphs induced by the adjacency matrices A_G and A_H in Definition B.1 are isomorphic to the original graphs G and H , respectively, and therefore they are also WL-indistinguishable. Additionally, we notice that the graphs induced by the adjacency matrices $A_{\mathcal{T}(G)}$ and $A_{\mathcal{T}(H)}$ in Definition B.1 are both isomorphic to the fully disconnected graph with 8 nodes, making them WL-indistinguishable as well. We also observe that there exists a bijection $\sigma : V_G \rightarrow V_H$ that maps all nodes of degree 3 in G to all nodes of degree 3 in H . The definition of $\mathcal{T}(\cdot)$ implies that σ is an isomorphism between the adjacency matrices A_{P_i} corresponding to G and H , where $i = 1, 2$. Finally, we notice that for both G , and H , the node feature map induced by π_S satisfies:

$$\mathcal{X}^{\pi_S}(S, v) = \deg(v) - 2. \quad (163)$$

This node feature map can be easily implemented by the layer update in definition B.2 and so it can be ignored. Since all four graphs corresponding to G that are induced by the adjacency matrices in Definition B.1, are WL-indistinguishable from their counterpart corresponding to H , and equation 29 in definition B.2 is an MPNN update, which is incapable of distinguishing graphs that are WL-indistinguishable, we see that equation 162 holds, concluding the proof. \square

Proposition C.3 (Node + Size Marking as Invariant Marking). *Given a graph $G = (V, E)$ with node feature vector $X \in \mathbb{R}^{n \times d}$, and a coarsening function $\mathcal{T}(\cdot)$, let $\mathcal{X}^{\pi_{ss}}, \mathcal{X}^{\pi_{inv}}$ be the node feature maps induced by π_{ss} and π_{inv} respectively. Recall that:*

$$\mathcal{X}^{\pi_{ss}}(S, v) = [X_v, b_{\pi_{ss}}(S, v)], \quad (43)$$

$$\mathcal{X}^{\pi_{inv}}(S, v) = [X_v, b_{\pi_{inv}}(S, v)]. \quad (44)$$

The following now holds:

$$b_{\pi_{inv}}(S, v) = \text{OHE}(b_{\pi_{ss}}(S, v)) \quad \forall S \in V^{\mathcal{T}}, \forall v \in V. \quad (45)$$

Here, OHE denotes a one-hot encoder, independent of the choice of both G and \mathcal{T} .

Proof. Let $G = (V, E)$ be a graph with $V = [n]$, and let $\mathcal{T}(\cdot)$ be a coarsening function. Recall that the maps $b_{\pi_{ss}}(\cdot, \cdot)$ and $b_{\pi_{inv}}(\cdot, \cdot)$ are both independent of the connectivity of G and are defined as follows:

$$b_{\pi_{ss}}(S, v) = \begin{cases} (1, |S|) & v \in S, \\ (0, |S|) & v \notin S. \end{cases} \quad (164)$$

$$b_{\pi_{inv}}(S, v) = [\mathbf{1}_{\gamma_1}(S, v), \dots, \mathbf{1}_{\gamma_k}(S, v)]. \quad (165)$$

Here, $v \in [n]$, $S \in \mathcal{T}([n]) \subseteq \mathcal{P}([n])$, $\gamma_1, \dots, \gamma_k$ is any enumeration of the set of all orbits $(\mathcal{P}([n]) \times [n])/S_n$, and $\mathbf{1}_{\gamma_i}$ denotes the indicator function of orbit γ_i . Since any tuple $(S, v) \in \mathcal{P}([n]) \times [n]$ belongs to exactly one orbit γ_i , we note that the right hand side of Equation (165) is a one-hot encoded vector. Thus, it suffices to show that for every $v, v' \in [n]$ and $S, S' \in \mathcal{P}([n])$, we have:

$$b_{\pi_{ss}}(S, v) = b_{\pi_{ss}}(S', v') \Leftrightarrow b_{\pi_{inv}}(S, v) = b_{\pi_{inv}}(S', v'). \quad (166)$$

This is equivalent to:

$$(\mathcal{P}([n]) \times [n])/S_n = \{(S, v) \mid |S| = i, \mathbf{1}_S(v) = j \mid i \in [n], j \in \{0, 1\}\}. \quad (167)$$

Essentially, this means that each orbit corresponds to a choice of the size of s and whether $v \in S$ or not. To conclude the proof, it remains to show that for any two pairs $(S, v), (S', v') \in \mathcal{P}([n]) \times [n]$, there exists a permutation $\sigma \in S_n$ such that:

$$\sigma \cdot (S, v) = (S', v') \quad (168)$$

if and only if

$$|S| = |S'| \text{ and } \mathbf{1}_S(v) = \mathbf{1}_{S'}(v'). \quad (169)$$

Assume first that $\sigma \cdot (S, v) = (S', v')$, then $\sigma^{-1}(S) = S'$ and since σ is a bijection, $|S| = |S'|$. In addition $\sigma^{-1}(v) = v'$ thus:

$$v \in S \Leftrightarrow v' = \sigma^{-1}(v) \in \sigma^{-1}(S) = S'. \quad (170)$$

Assume now that:

$$|S| = |S'| \quad (171)$$

$$\mathbf{1}_S(v) = \mathbf{1}_{S'}(v') \quad (172)$$

It follows that for some $r, m \in [n]$:

$$|S \setminus \{v\}| = |S' \setminus \{v'\}| = r \quad \text{and} \quad |[n] \setminus (S \cup \{v\})| = |[n] \setminus (S' \cup \{v'\})| = m \quad (173)$$

Write:

$$\begin{aligned} S \setminus \{v\} &= \{i_1, \dots, i_r\}, & S' \setminus \{v'\} &= \{i'_1, \dots, i'_r\}, \\ [n] \setminus (S \cup \{v\}) &= \{j_1, \dots, j_m\}, & [n] \setminus (S' \cup \{v'\}) &= \{j'_1, \dots, j'_m\} \end{aligned}$$

and define:

$$\sigma(x) = \begin{cases} v' & x = v \\ i'_l & x = i_l, l \in [r] \\ j'_l & x = j_l, l \in [m] \end{cases} \quad (174)$$

We now have:

$$\sigma \cdot (S, v) = (S', v'). \quad (175)$$

This concludes the proof. \square

G.3 Proofs of Appendix D.1

Proposition D.1 (CS-GNN Can Implement MSGNN). *Let $\mathcal{T}(\cdot)$ be the identity coarsening function defined by:*

$$\mathcal{T}(G) = \{\{v\} \mid v \in V\} \quad \forall G = (V, E). \quad (49)$$

The following holds:

$$CS\text{-}GNN(\mathcal{T}, \pi_S) = MSGNN(\pi_{NM}). \quad (50)$$

Proof. Abusing notation, for a given graph $G = (V, E)$ we write $\mathcal{T}(G) = G$, $V^\mathcal{T} = V$. First, we observe that:

$$v \in \{u\} \Leftrightarrow u = v, \quad (176)$$

This implies that the initial node feature map $\mathcal{X}^0(u, v)$ induced by π_S is equivalent to the standard node marking described in equation 46. Additionally, we note that the pooling procedures for both models, as described in equations 16 and 55, are identical. Therefore, it is sufficient to show that the CS-GNN and MSGNN layer updates described in equations 15 and 47 respectively are also identical. For this purpose, let $\mathcal{X}^t(v, u)$ be a node feature map supported on the set $V \times V$. The inputs to the MSGNN layer are the following:

1. $\mathcal{X}^t(u, v)$.
2. $\mathcal{X}^t(u, u)$.
3. $\mathcal{X}^t(v, v)$.
4. $\text{agg}_1^t \{ \{ \mathcal{X}^t(u, v'), e_{v, v'} \} \mid v' \sim v \}$.
5. $\text{agg}_2^t \{ \{ \mathcal{X}^t(u', v), e_{u, u'} \} \mid u' \sim u \}$.

The inputs to the CS-GNN layer are the following:

1. $\mathcal{X}^t(S, v) \Rightarrow \mathcal{X}^t(u, v)$.
2. $\text{agg}_1^t \{ \{ \mathcal{X}^t(S, v'), e_{v, v'} \} \mid v' \sim_G v \} \Rightarrow \text{agg}_1^t \{ \{ \mathcal{X}^t(u, v'), e_{v, v'} \} \mid v' \sim v \}$.
3. $\text{agg}_2^t \{ \{ \mathcal{X}^t(S', v), \tilde{e}_{S, S'} \} \mid S' \sim_{G^\mathcal{T}} S \} \Rightarrow \text{agg}_2^t \{ \{ \mathcal{X}^t(u, u'), e_{u, v'} \} \mid v' \sim v \}$.
4. $\text{agg}_3^t \{ \{ \mathcal{X}^t(S', v), z(S, v, S', v) \} \mid \forall s' \in V^\mathcal{T} \text{ s.t. } v \in S' \} \Rightarrow \{ \{ X^t(v, v), z(u, v, v, v) \} \}$.
5. $\text{agg}_4^t \{ \{ \mathcal{X}^t(S, v'), z(S, v, S, v') \} \mid \forall u' \in V \text{ s.t. } v' \in S \} \Rightarrow \{ \{ X^t(u, u), z(u, v, u, u) \} \}$.

The terms $z(u, v, v, v)$ and $z(u, v, u, u)$ appearing in the last two input terms of the CS-GNN layer uniquely encode the orbit tuples (u, v, v, v) and (u, v, u, u) belong to respectively. Since these orbits depend solely on whether $u = v$, these values are equivalent to the node marking feature map $\mathcal{X}^0(u, v)$. Therefore, these terms can be ignored. Observing the two lists above, we see that the inputs to both update layers are identical (ignoring the $z(\cdot)$ terms). Thus, as both updates act on these inputs in the same way, the updates themselves are identical. and so

$$MSGNN(\pi_{NM}) = CS\text{-}GNN(\mathcal{T}, \pi_S). \quad (177)$$

□

G.4 Proofs of Appendix D.2

Proposition D.2 (CS-GNN Is at Least as Expressive as Coarse MPNN). *For any coarsening function $\mathcal{T}(\cdot)$ the following holds:*

$$MPNN \subseteq MPNN_+(\mathcal{T}) \subseteq CS\text{-}GNN(\mathcal{T}, \pi_S) \quad (58)$$

Proof. For convenience, let us first restate the CS-GNN layer update:

$$\begin{aligned}\mathcal{X}^{t+1}(S, v) = f^t \Big(& \mathcal{X}^t(S, v), \\ & \text{agg}_1^t \{ \{ \mathcal{X}^t(S, v'), e_{v, v'} \} \mid v' \sim_G v \}, \\ & \text{agg}_2^t \{ \{ \mathcal{X}^t(S', v), \tilde{e}_{S, S'} \} \mid S' \sim_{G^\tau} S \}, \\ & \text{agg}_3^t \{ \{ \mathcal{X}^t(S', v), z(S, v, S', v) \} \mid S' \in V^\tau \text{ s.t. } v \in S' \}, \\ & \text{agg}_4^t \{ \{ \mathcal{X}^t(S, v'), z(S, v, S, v') \} \mid u' \in V \text{ s.t. } v' \in S \} \Big),\end{aligned}\tag{15}$$

as well as the MPNN₊ layer update:

$$\begin{aligned}\text{For } v \in V : \quad & \mathcal{X}^{t+1}(v) = f_V^t \left(\mathcal{X}^t(v), \text{agg}_1^t \{ \{ \mathcal{X}^t(v'), e_{v, v'} \} \mid v \sim_G v' \}, \right. \\ & \left. \text{agg}_2^t \{ \{ \mathcal{X}^t(S) \mid S \in V^\tau, v \in S \} \}, \right) \\ \text{For } S \in V^\tau : \quad & \mathcal{X}^{t+1}(S) = f_{V^\tau}^t \left(\mathcal{X}^t(S), \text{agg}_1^t \{ \{ \mathcal{X}^t(S'), e_{S, S'} \} \mid S \sim_{G^\tau} S' \}, \right. \\ & \left. \text{agg}_2^t \{ \{ \mathcal{X}^t(v) \mid v \in V, v \in S \} \} \right).\end{aligned}\tag{54}$$

We note that by setting $f_{V^\tau}^t$ to be a constant zero and choosing f_V^t to be any continuous function that depends only on its first two arguments, the update in equation 54 becomes a standard MPNN layer. This proves:

$$\text{MPNN} \subseteq \text{MPNN}_+(T).\tag{178}$$

Next, we prove the following 2 Lemmas:

Lemma G.1. *Given a graph $G = (V, E)$ such that $V = [n]$ with node feature vector $X \in \mathbb{R}^{n \times d}$, and a coarsening function $\mathcal{T}(\cdot)$, there exists a CS-GNN(\mathcal{T}, π_S) layer such that:*

$$\mathcal{X}^1(S, v) = [0_{d+1}, X_v, 1] = [\tilde{\mathcal{X}}^0(S), \tilde{\mathcal{X}}^0(v)].\tag{179}$$

Here $[\cdot, \cdot]$ denotes concatenation and $\tilde{\mathcal{X}}^0(\cdot)$ denotes the initial node feature map of the coarsened sum graph G_+^T .

Lemma G.2. *Let $\tilde{\mathcal{X}}^t(\cdot)$ denote the node feature maps of G_+^T at layers t of a stack of MPNN₊(\mathcal{T}) layers. There exists a stack of $t + 1$ CS-GNN(\mathcal{T}, π_S) layers such that:*

$$\mathcal{X}^{t+1}(S, v) = [\tilde{\mathcal{X}}^t(S), \tilde{\mathcal{X}}^t(v)].\tag{180}$$

proof of Lemma G.1. Recall that the initial node feature map of CS-GNN(\mathcal{T}, π_S) is given by:

$$\mathcal{X}^0(S, v) = \begin{cases} [X_v, 1] & v \in S \\ [X_v, 0] & v \notin S. \end{cases}\tag{181}$$

In addition, the initial node feature map of MPNN₊(\mathcal{T}) is given by:

$$\tilde{\mathcal{X}}^0(v) = \begin{cases} [X_v, 1] & v \in V \\ 0_{d+1} & v \in V^\tau. \end{cases}\tag{182}$$

Thus, we choose a layer update as described in equation 15 with:

$$\mathcal{X}^1(S, v) = f^0(\mathcal{X}^0(S, v), \cdot, \cdot, \cdot, \cdot) = [0_{d+1}, \mathcal{X}^0(S, v)_{1:d}, 1]\tag{183}$$

Here, $f(a, \cdot, \cdot, \cdot, \cdot)$ denotes that the function depends only on the parameter a , and $X_{a:b}$ indicates that only the coordinates a through b of the vector X are taken. This gives us:

$$\mathcal{X}^1(S, v) = [\tilde{\mathcal{X}}^0(S), \tilde{\mathcal{X}}^0(v)].\tag{184}$$

□

proof of Lemma G.2. We prove this Lemma by induction on t . We note that Lemma G.1 provides the base case $t = 0$. Assume now that for a given stack of $t + 1$ $\text{MPNN}_+(\mathcal{T})$ layer updates, with corresponding node feature maps:

$$\tilde{\mathcal{X}}^i : V_+^{\mathcal{T}} \rightarrow \mathbb{R}^{d_i} \quad i = 1 \dots, t + 1, \quad (185)$$

there exists a stack of $t + 1$ $\text{CS-GNN}(\mathcal{T}, \pi_S)$ layers with node feature maps:

$$\mathcal{X}^i : V^{\mathcal{T}} \times V \rightarrow \mathbb{R}^{2d_i} \quad i = 1, \dots, t + 1, \quad (186)$$

such that:

$$\mathcal{X}^{t+1}(S, v) = [\tilde{\mathcal{X}}^t(S), \tilde{\mathcal{X}}^t(v)]. \quad (187)$$

We shall show that there exists a single additional $\text{CS-GNN}(\mathcal{T}, \pi_S)$ layer update such that:

$$\mathcal{X}^{t+2}(S, v) = [\tilde{\mathcal{X}}^{t+1}(S), \tilde{\mathcal{X}}^{t+1}(v)]. \quad (188)$$

For that purpose we define the following $\text{CS-GNN}(\mathcal{T}, \pi_S)$ update (abusing notation, the left hand side refers to components of the $\text{CS-GNN}(\mathcal{T}, \pi_S)$ update at layer $t + 1$, while the right hand side refers to components of the $\text{MPNN}_+(\mathcal{T})$ update at layer t):

$$\begin{aligned} \text{agg}_1^{t+1} &= \text{agg}_1^t|_{1:d_t}, \\ \text{agg}_2^{t+1} &= \text{agg}_1^t|_{d_t+1:2d_t}, \\ \text{agg}_3^{t+1} &= \text{agg}_2^t|_{1:d_t}, \\ \text{agg}_4^{t+1} &= \text{agg}_2^t|_{d_t+1:2d_t}, \end{aligned} \quad (189)$$

$$f^{t+1}(a, b, c, d, e) = [f_V^t(a_{1:d_t}, b, d), f_{V^{\mathcal{T}}}^t(a_{d_t+1:2d_t}, c, e)]. \quad (190)$$

Here the operation $\text{agg}_{a:b}$ initially projects all vectors in the input multi-set onto coordinates a through b , and subsequently passes them to the function agg . equations 189 , 190 guarantee that:

$$\begin{aligned} \mathcal{X}^{t+2}(S, v)_{1:d_{t+1}} &= f_V^t(\mathcal{X}^t(S, v)_{1:d_t}, \\ &\quad \text{agg}_1^t\{(S, v')_{1:d_t} \mid v \sim_G v'\}, \\ &\quad \text{agg}_2^t\{(S', v)_{1:d_t} \mid v \in S'\}) \\ &= \tilde{\mathcal{X}}^{t+1}(v), \\ \mathcal{X}^{t+2}(S, v)_{d_{t+1}+1:2d_{t+1}} &= f_{V^{\mathcal{T}}}^t(\mathcal{X}^t(S, v)_{d_t+1:2d_t}, \\ &\quad \text{agg}_1^t\{(S', v)_{d_t+1:2d_t} \mid S' \sim_{\mathcal{T}(G)} S\}, \\ &\quad \text{agg}_2^t\{(S, v')_{d_t+1:2d_t} \mid v' \in S\}) \\ &= \tilde{\mathcal{X}}^{t+1}(S). \end{aligned} \quad (191)$$

This proves the Lemma. \square

Now, for a given finite family of graphs \mathcal{G} and a function $f \in \text{MPNN}_+(\mathcal{T})$, there exists a stack of T $\text{MPNN}_+(\mathcal{T})$ layers such that:

$$f(G) = U \left(\sum_{v \in V_+^{\mathcal{T}}} \tilde{\mathcal{X}}^T(v) \right) \quad \forall G \in \mathcal{G}. \quad (192)$$

Here, $\tilde{\mathcal{X}}^T : V_+^{\mathcal{T}} \rightarrow \mathbb{R}^{d_T}$ denotes the final node feature map, and U is an MLP. Lemma G.2 now tells us that there exists a stack of $T + 1$ $\text{CS-GNN}(\mathcal{T}, \pi_S)$ layers such that:

$$\mathcal{X}^{T+1}(S, v) = [\tilde{\mathcal{X}}^T(S), \tilde{\mathcal{X}}^T(v)]. \quad (193)$$

Similarly to Lemma G.1, we use one additional layer to pad $\mathcal{X}^{T+1}(S, v)$ as follows:

$$\mathcal{X}^{T+2}(S, v) = [\tilde{\mathcal{X}}^T(S), \tilde{\mathcal{X}}^T(v), 1]. \quad (194)$$

We notice that:

$$\begin{aligned}\sum_{s \in V^T} \mathcal{X}^{T+2}(S, v) &= \left[\sum_{S \in V^T} \tilde{X}^T(S), \sum_{S \in V^T} \tilde{X}^T(v), \sum_{S \in V^T} 1 \right] \\ &= \left[\sum_{S \in V^T} \tilde{X}^T(S), |V^T| \cdot \tilde{X}^T(v), |V^T| \right].\end{aligned}\quad (195)$$

Thus, in order to get rid of the $|V^T|$ term, We define:

$$\text{MLP}_1(a, b, c) = [a, \frac{1}{c} \cdot b, 1], \quad a, b \in \mathbb{R}^{d_L}, c > 0. \quad (196)$$

We note that since we are restricted to a finite family of input graphs, the use of an MLP in equation 199 can be justified using Theorem G.1 (see the proof of Proposition B.1 for a detailed explanation).

Equations 195 and 199 imply:

$$\text{MLP}_1 \left(\sum_{s \in V^T} \mathcal{X}^{T+2}(S, v) \right) = \left[\sum_{S \in V^T} \tilde{X}^T(S), \tilde{X}^T(v), 1 \right] \quad (197)$$

Thus, similarly to equation 195:

$$\sum_{v \in V} \text{MLP}_1 \left(\sum_{S \in V^T} \mathcal{X}^{T+2}(S, v) \right) = \left[|V| \cdot \sum_{S \in V^T} \tilde{X}^T(S), \sum_{v \in V} \tilde{X}^T(v), |V| \right] \quad (198)$$

And so, in order to get rid of the $|V|$ term, We define:

$$\text{MLP}_2(a, b, c) = U(a \cdot \frac{1}{c} + b, 1), \quad a, b \in \mathbb{R}^{d_T}, c > 0. \quad (199)$$

Thus for all $G \in \mathcal{G}$:

$$\begin{aligned}\text{MLP}_2 \left(\sum_{v \in V} \text{MLP}_1 \left(\sum_{S \in V^T} \mathcal{X}^{T+2}(S, v) \right) \right) \\ &= \text{MLP}_2 \left(\left[|V| \cdot \sum_{S \in V^T} \tilde{X}^T(S), \sum_{v \in V} \tilde{X}^T(v), |V| \right] \right) \\ &= U \left(\sum_{v \in V_+^T} \tilde{X}^T(v) \right) \\ &= f(G).\end{aligned}\quad (200)$$

and so $f \in \text{CS-GNN}(\mathcal{T}, \pi_S)$. This proves:

$$\text{MPNN}_+(T) \subseteq \text{CS-GNN}(\mathcal{T}, \pi_S). \quad (201)$$

□

Proposition D.3 (CS-GNN Can Be More Expressive Than MPNN+). *Let $\mathcal{T}(\cdot)$ be the identity coarsening function defined by:*

$$\mathcal{T}(G) = \{\{v\} \mid v \in V\} \quad G = (V, E). \quad (59)$$

The following holds:

$$\text{MPNN} = \text{MPNN}_+(\mathcal{T}). \quad (60)$$

Thus:

$$\text{MPNN}_+(\mathcal{T}) \subset \text{CS-GNN}(\mathcal{T}, \pi_S), \quad (61)$$

where this containment is strict.

Proof. First, using the notation \tilde{v} to mark the single element set $\{v\} \in V^\mathcal{T}$, We notice that the $\text{MPNN}_+(\mathcal{T})$ layer update described in equation 54, becomes:

$$\begin{aligned} \text{For } v \in V : \quad \mathcal{X}^{t+1}(v) &= f_V^t \left(\mathcal{X}^t(v), \mathcal{X}^t(\tilde{v}), \text{agg}^t \left\{ \left(\mathcal{X}^t(v'), e_{v,v'} \right) \mid v' \sim_G v \right\} \right), \\ \text{For } \tilde{v} \in V^\mathcal{T} : \quad \mathcal{X}^{t+1}(\tilde{v}) &= f_{V^\mathcal{T}}^t \left(\mathcal{X}^t(\tilde{v}), \mathcal{X}^t(v), \text{agg}^t \left\{ \left(\mathcal{X}^t(\tilde{v}'), e_{\tilde{v},\tilde{v}'} \right) \mid v \sim_G v' \right\} \right). \end{aligned} \quad (202)$$

Now, for a given finite family of graphs \mathcal{G} and a function $f \in \text{MPNN}_+(\mathcal{T})$, there exists a stack of T $\text{MPNN}_+(\mathcal{T})$ layers such that:

$$f(G) = U \left(\sum_{v \in V_+^\mathcal{T}} \mathcal{X}^T(v) \right) \quad \forall G \in \mathcal{G}. \quad (203)$$

Here, $\mathcal{X}^T : V_+^\mathcal{T} \rightarrow \mathbb{R}^d$ denotes the final node feature map, and U is an MPL. We now prove by induction on t that there exists a stack of t standard MPNN layers, with corresponding node feature map $X^t : V \rightarrow \mathbb{R}^{2d_t}$ such that :

$$X^t(v) = [\mathcal{X}^t(v), \mathcal{X}^t(\tilde{v})]. \quad (204)$$

Here, $[\cdot, \cdot]$ stands for concatenation. We assume for simplicity that the input graph G does not have node features, though the proof can be easily adapted for the more general case. We notice that for the base case $t = 0$, equation 53 in definition D.2 implies:

$$\mathcal{X}^0(v) = \begin{cases} 1 & v \in V, \\ 0 & v \in V^\mathcal{T}. \end{cases} \quad (205)$$

Thus, we define:

$$X^0(v) = (1, 0). \quad (206)$$

This satisfies Equation (204), establishing the base case of the induction. Assume now that Equation (204) holds for some $t \in [T]$. Let $\text{agg}^t, f_V^t, f_{V^\mathcal{T}}^t$ be the components of layer t , as in equation 202. We define:

$$\text{agg}^t = [\text{agg}^t|_{1:d_t}, \text{agg}^t|_{d_t+1:2d_t}]. \quad (207)$$

Here the operation $\text{agg}|_{a:b}$ initially projects all vectors in the input multi-set onto coordinates a through b , and subsequently passes them to the function agg .

Additionally, let d^* denote the dimension of the output of the function agg^t . We define:

$$\tilde{f}^t(a, b) = [f_V^t(a|_{1:d_t}, a|_{d_t+1:2d_t}, b|_{1:d^*}), f_{V^\mathcal{T}}^t(a|_{d_t+1:2d_t}, a|_{1:d_t}, b|_{d^*+1:2d^*})]. \quad (208)$$

Finally, we update our node feature map X^t using a standard MPNN update according to:

$$X^{t+1}(v) = \tilde{f}^t(X^t(v), \left\{ (X^t(v'), e_{v,v'}) \mid v' \sim_G v \right\}). \quad (209)$$

equations 202, 204 and 209 now guarantee that:

$$X^{t+1}(v) = [\mathcal{X}^t(v), \mathcal{X}^{t+1}(\tilde{v})]. \quad (210)$$

This concludes the inductive proof. We now define:

$$\text{MLP}(x) = U(x|_{1:d_T}) + U(x|_{d_T+1:2d_T}). \quad (211)$$

This gives us:

$$U \left(\sum_{v \in V_+^\mathcal{T}} \mathcal{X}^T(v) \right) = \text{MLP} \left(\sum_{v \in V} X^T(v) \right) = f(G). \quad (212)$$

We have thus proven that $f \in \text{MPNN}$ and so:

$$\text{MPNN}_+(\mathcal{N}) \subseteq \text{MPNN}. \quad (213)$$

Combining this result with Proposition D.2, we obtain:

$$\text{MPNN} = \text{MPNN}_+(\mathcal{T}). \quad (214)$$

Finally, since Proposition D.1 tells us that $\text{CS-GNN}(\mathcal{T}, \pi_S)$ has the same implementation power as the maximally expressive node policy subgraph architecture MSGNN, which is proven to be strictly more expressive than the standard MPNN, we have:

$$\text{MPNN}_+(\mathcal{T}) \subset \text{CS-GNN}(\mathcal{T}, \pi_S). \quad (215)$$

□

Lemma E.1 (γ (Γ) are orbits). *The sets $\{\gamma^{k*} : k = 1, \dots, n; * \in \{+, -\}\}$ and $\{\Gamma^{\leftrightarrow; k_1; k_2; k^\cap; \delta_{\text{same}}; \delta_{\text{diff}}}\}$ are the orbits of S_n on the index space $(\mathcal{P}([n]) \times [n])$ and $(\mathcal{P}([n]) \times [n] \times (\mathcal{P}([n]) \times [n]))$, respectively.*

Proof. We will prove this lemma for γ . The proof for Γ follows similar reasoning; we also refer the reader to [22] for a general proof.

We will prove this lemma through the following three steps.

- (1). Given indices $(S, i) \in \mathcal{P}([n]) \times [n]$, there exists $\gamma \in (\mathcal{P}([n]) \times [n])_\sim$ such that $(S, i) \in \gamma$.
- (2). Given indices $(S, i) \in \gamma$, for any $\sigma \in S_n$, it holds that $(\sigma^{-1}(S), \sigma^{-1}(i)) \in \gamma$.
- (3). Given $(S, i) \in \gamma$ and $(S', i') \in \gamma$ (the same γ), it holds that there exists a $\sigma \in S_n$ such that $\sigma \cdot (S, i) = (S', i')$.

We prove in what follows.

(1). Given indices $(S, i) \in \mathcal{P}([n]) \times [n]$, w.l.o.g. we assume that $|S| = k$, thus if $i \in S$ ($i \notin S$) it holds that $(S, i) \in \gamma^{k-}$ ($(S, i) \in \gamma^{k+}$), recall Equation (70).

(2). Given indices $(S, i) \in \gamma$, note that any permutation $\sigma \in S_n$ does not change the cardinality of S nor the inclusion (or exclusion) of i in S . Recalling Equation (70), we complete this step.

(3). Given that $(S, i) \in \gamma$ and $(S', i') \in \gamma$, and recalling Equation (70), we note that $|S| = |S'|$ and that either both $i \in S$ and $i' \in S'$, or both $i \notin S$ and $i' \notin S'$.

(3.1). In (3.1) we focus on the case where $i \notin S$ and $i' \notin S'$. Let $S = \{i_1, \dots, i_k\}$ and $S' = \{i'_1, \dots, i'_k\}$. Then, we have $(\{i_1, \dots, i_k\}, j)$ and $(\{i'_1, \dots, i'_k\}, j')$. Define $\sigma \in S_n$ such that $\sigma(i_l) = i'_l$ for $l \in [k]$, and $\sigma(j) = j'$. Since $(\{i_1, \dots, i_k\}, j)$ consists of $k+1$ distinct indices and $(\{i'_1, \dots, i'_k\}, j')$ also consists of $k+1$ distinct indices, this is a valid $\sigma \in S_n$.

(3.2). Here, we focus on the case where $i \in S$ and $i' \in S'$. This proof is similar to (3.1), but without considering the indices j and j' , as they are included in S and S' , respectively.

□

Proposition E.1 (Basis of Invariant (Equivariant) Layer). *The tensors \mathbf{B}^γ (\mathbf{B}^Γ) in Equation (71) (Equation (73)) form an orthogonal basis (in the standard inner product) to the solution of Equation (65) (Equation (66)).*

Proof. We prove this proposition for the invariant case. The equivariant case is proved similarly – we also refer the reader for [22] for a general proof. We will prove this in three steps,

- (1). For any $\gamma \in (\mathcal{P}([n]) \times [n])_\sim$ it holds that $\mathbf{B}_{S,i}^\gamma$ solves Equation (65).
- (2). Given a solution \mathbf{L} to Equation (65), it is a linear combination of the basis elements.
- (3). We show that the basis vectors are orthogonal and thus linearly independent.

We prove in what follows.

(1). Given $\gamma \in (\mathcal{P}([n]) \times [n])_\sim$, we need to show that $\mathbf{B}_{S,i}^\gamma = \mathbf{B}_{\sigma^{-1}(S), \sigma^{-1}(i)}^\gamma$. Since any $\gamma \in (\mathcal{P}([n]) \times [n])_\sim$ is an orbit in the index space (recall Lemma E.1), and $\mathbf{B}_{S,i}^\gamma$ are indicator vectors of the orbits this always holds.

(2). Given a solution \mathbf{L} to Equation (65), it must hold that $\mathbf{L}_{S,i} = \mathbf{L}_{\sigma^{-1}(S), \sigma^{-1}(i)}$. Since the set $\{\gamma^{k*} : k = 1, \dots, n; * \in \{+, -\}\}$ corresponds to the orbits in the index space with respect to S_n , \mathbf{L} should have the same values over the index space of these orbits. Let's define these values as α^γ for each $\gamma \in \{\gamma^{k*} : k = 1, \dots, n; * \in \{+, -\}\}$. Thus, we obtain that $\mathbf{L}' = \sum_{\gamma \in (\mathcal{P}([n]) \times [n])_\sim} \alpha^\gamma \cdot \mathbf{B}^\gamma$, since \mathbf{B}^γ are simply indicator vectors of the orbits. This completes this step.

(3). Once again, since the basis elements are indicator vectors of disjoint orbits we obtain their orthogonality, and thus linearly independent. \square